Resilient Cities and Structures 4 (2025) 16–40

Contents lists available at ScienceDirect

Resilient Cities and Structures

journal homepage: www.elsevier.com/locate/rcns

Full Length Article

An integrated decision-making approach to resilience–LCC Bridge network retrofitting using a genetic algorithm-based framework

Pedram Omidian [a], Naser Khaji [b,*], Ali Akbar Aghakouchak [a]

[a] Faculty of Civil and Environmental Engineering, Tarbiat Modares University, P.O. Box 14115–397, Tehran, Iran
[b] Civil and Environmental Engineering Program, Graduate School of Advanced Science and Engineering, Hiroshima University, 1-4-1, Kagamiyama, Higashi-Hiroshima, Hiroshima 739-8527, Japan

ARTICLE INFO

Keywords:
Bridge network
Infrastructures management
Decision-making framework
Resilience
Life-cycle cost

ABSTRACT

Bridge networks are essential components of civil infrastructure, supporting communities by delivering vital services and facilitating economic activities. However, bridges are vulnerable to natural disasters, particularly earthquakes. To develop an effective disaster management strategy, it is critical to identify reliable, robust, and efficient indicators. In this regard, Life-Cycle Cost (LCC) and Resilience (R) serve as key indicators to assist decision-makers in selecting the most effective disaster risk reduction plans. This study proposes an innovative LCC–R optimization framework to identify the most optimal retrofit strategies for bridge networks facing hazardous events during their lifespan. The proposed framework employs both single- and multi-objective optimization techniques to identify retrofit strategies that maximize the R index while minimizing the LCC for the under-study bridge networks. The considered retrofit strategies include various options such as different materials (steel, CFRP, and GFRP), thicknesses, arrangements, and timing of retrofitting actions. The first step in the proposed framework involves constructing fragility curves by performing a series of nonlinear time-history incremental dynamic analyses for each case. In the subsequent step, the seismic resilience surfaces are calculated using the obtained fragility curves and assuming a recovery function. Next, the LCC is evaluated according to the proposed formulation for multiple seismic occurrences, which incorporates the effects of complete and incomplete repair actions resulting from previous multiple seismic events. For optimization purposes, the Non-Dominated Sorting Genetic Algorithm II (NSGA-II) evolutionary algorithm efficiently identifies the Pareto front to represent the optimal set of solutions. The study presents the most effective retrofit strategies for an illustrative bridge network, providing a comprehensive discussion and insights into the resulting tactical approaches. The findings underscore that the methodologies employed lead to logical and actionable retrofit strategies, paving the way for enhanced resilience and cost-effectiveness in bridge network management against seismic hazards.

1. Introduction

As social and economic conditions have gradually improved, the approach to urban construction is shifting from rapid expansion to a focus on high-quality development. In addition, over time, there has been a significant increase in population density, the availability of medical resources, and overall socio-economic development. In this regard, lifeline systems are critical in providing essential services and supporting economic activities. However, civil infrastructure systems, including ground transportation networks, are highly vulnerable to natural disasters such as earthquakes [1]. These disasters may eventually lead to structural collapse and negatively impact the community and the economy. As integral components of transportation networks, bridges play a vital role in various socio-economic activities, such as logistics, emergency medical services, and search and rescue operations in urban areas [2]. The functional losses of bridges can lead to mobility limitations and increased user costs, which emphasizes the need for their robustness and efficient pre- and post-disaster measures. In this line, prioritizing rehabilitation/retrofitting interventions is crucial for restoring/maintaining the overall serviceability of the transportation network. For this reason, effective and dynamic decision-making frameworks must be used to correctly model interdependencies/dependencies, expected risks, and uncertainties that take into account logical indicators [3].

In infrastructure management, the Life-Cycle Cost Analysis (LCCA) can be utilized to find the most effective strategies for mitigating seismic hazard risks [4]. The LCCA, as a monetary risk indicator, is widely recognized as a powerful method for quantitatively analyzing bridge seismic risks by considering the potential losses resulting from earthquake events. In this respect, the Life-Cycle Cost (LCC) means consider-

* Corresponding author.
E-mail address: nkhaji@hiroshima-u.ac.jp (N. Khaji).

https://doi.org/10.1016/j.rcns.2024.12.002
Received 29 August 2024; Received in revised form 11 December 2024; Accepted 25 December 2024
Available online 7 January 2025

ing all the costs, including an initial investment (typically design and construction costs), ongoing expenses (such as maintenance, retrofit and repair costs or renewal/replacement costs), and demolition costs [5]. Wang et al. [6] developed a simplified decision-making framework to calculate seismic loss and assess the life-cycle cost of base-isolated-reinforced concrete structure. Shekhar and Ghosh [7] suggested a multi-dimensional function framework to estimate the LCC and vulnerability of structurally dissimilar highway bridges using parameterized fragility models in regions with moderate to high seismicity. Torti et al. [8] introduced a novel combined model of LCC formulation and simulation methodology for the long-term financial evaluation of transportation bridges equipped with seismic structural health monitoring systems. In this regard, research has been conducted on developing methodologies for life-cycle cost analysis to determine the most effective managing strategy for infrastructure systems exposed to extreme natural disasters [9]. As evidenced in most of the LCCA research, there are two potential repair scenarios for a given damage state of a structure: (I) completing the repair actions before the next hazard event and allowing the structure to return to its original state, or (II) assuming that repair actions are not finished before subsequent events, which could exacerbate the existing damage condition due to the following hazardous events. In this line, while the LCCA can consider a structure's performance, indicators such as Resilience (R) offer insights into the functionality level of infrastructure and its ability to recover and return to its pre-event performance [10].

Resilience is increasingly central in designing, assessing, monitoring, maintaining, and managing infrastructure systems. Resilience can be defined as the ability of a system to withstand the effects of disruptive events and efficiently recover to pre-event performance. In this connection, many research studies have focused on developing methodologies to evaluate the resilience of infrastructure systems [11]. Lu et al. [12] proposed a bi-level resource allocation framework to enhance the resilience of at-risk bridges in a transportation network by incorporating cost-effective retrofit strategies. In this context, Patel et al. [13] created a three-level hierarchical structure that combines the bridge resilience index at the 1st level, 4Rs (i.e., Robustness, Rapidity, Resourcefulness, and Redundancy) at the 2nd level, and TOSE (i.e., Technical, Organizational, Social, and Economical) dimension factors at the 3rd level. Rasulo et al. [14] proposed a model to evaluate the resilience of road networks after an earthquake due to bridge damage and restoration activities by assessing the impact of earthquake-induced disruptions on transportation capacities, traffic congestion, and travel times. In addition, several research studies have been carried out to simultaneously integrate and compare different risk indicators within a single framework [15–18]. Omidian and Khaji [19] proposed a resilience–cost of retrofit optimization framework for improving the seismic resilience of Reinforced Concrete (RC) structures using Non-dominated Sorting Genetic Algorithm-II (NSGA-II).

Policymakers must develop disaster risk reduction methodologies to find the most optimal mitigation strategies in infrastructure management. In this regard, this research proposes a logical and practical optimization framework by examining and comparing various objectives, such as the life-cycle cost, retrofit cost, and resilience index, through single- or multi-objective optimization. This framework presents a comprehensive understanding of the current and future states of the understudy system, enabling decision-makers to make informed decisions on how to effectively manage infrastructure throughout its life-cycle. To demonstrate the proposed framework, an illustrative bridge network with different site seismicity is used as a case study infrastructure. In this line, each bridge is considered an RC box girder bridge with different pier retrofit strategies. These strategies include ten different timeframes of retrofitting action, eight retrofitting arrangements, and three materials with four different thicknesses (namely, steel, Glass Fiber Reinforced Polymer (GFRP) and Carbon Fiber Reinforced Polymer (CFRP)). The first step in the proposed framework is to construct the fragility curves by performing a series of Nonlinear Time-History Incremental Dynamic Analysis (NTH-IDA) for each case. These fragility curves are then used to calculate the seismic resilience curves/surfaces by assuming recovery function. In the following step, the life-cycle cost is determined based on the fragility and hazard curves with multiple seismic events, considering the impact of the finished/unfinished repair interventions. The implemented LCC formulation for the existing structure includes three costs: (1) the life-cycle repair cost (including all direct and indirect life-cycle costs resulting from hazardous events), (2) the life-cycle maintenance cost, and (3) the cost of retrofit during its service lifetime. In the last step, the NSGA-II, a widely recognized and efficient evolutionary algorithm for multi-objective optimization, has been implemented in the MATLAB platform [20]. The algorithm is aimed to identify the Pareto front, which represents the optimal set of solutions, by minimizing the LCC (or the cost of retrofit) and maximizing the resilience index. The flowchart of the optimization framework procedure of this study is presented in Fig. 1.

2. Theoretical foundations of resilience

Resilience, $R(t)$, refers to the capacity of infrastructure to withstand and recover from hazardous events, as assessed by a predetermined level of functionality, $Q(t)$, within a control time (T_{LC}) [21]. The resilience concept can be calculated as a non-stationary stochastic process with a piecewise continuous function based on research in different infrastructure systems [22]. Mathematically, the resilience index can be defined as follows:

$$R(t) = \int_{t_{0E}}^{t_{0E}+T_{LC}} \frac{Q(t)}{T_{LC}} dt \tag{1}$$

To evaluate the system functionality, $Q(t)$, after an extreme event like an earthquake, it is imperative to consider two critical parameters of loss and recovery functions during the periods of disruption. Mathematically, this notion can be denoted as:

$$Q(t) = 100\% - \left[L\left(I,\ T_{RE}\right) \times \left\{H\left(t - t_{0E}\right) - H\left(t - \left(t_{0E} + T_{RE}\right)\right)\right\} \times f_{rec}\left(t,\ t_{0E},\ T_{RE}\right)\right] \tag{2}$$

where $L(I,\ T_{RE})$ is employed to depict the loss function concerning the intensity of the hazard (I) and the passage of time required to restore (T_{RE}). Furthermore, f_{rec} is the post-event restoration path, and $H(\cdot)$ presents the Heaviside step functions (also known as the unit step function). For an ideally serviceable and intact state, the system functionality $Q(t)$ is deemed to be 100 % (equal to $R(t) = 100\%$). Based on the same argument, system functionality declines when the system is damaged ($0 < Q(t) < 100\%$). To assess the robustness (or resilience at t_{OE}; R_0), it is necessary to quantify the loss of functionality at this time (Q_0). Consequently, the resilience index after an event, R_0, can be determined by a dimensionless cost as ($\frac{\text{Cost of repair}}{\text{Replacement cost}}$) based on the following relationship:

$$R_0(\%) = Q_0 = 100\% - \sum_k P_E\left(LS_k\right).r_k \tag{3}$$

in which $P_E(LS_k)$ refers to the kth limit state of under-study structure (i.e., slight, moderate, extensive, and complete), which can be derived from fragility curves [23,24]. Additionally, r_k is the damage ratio associated with the kth limit state [25].

It is essential to recognize that certain repair activities must be defined to restore the bridge via a specific recovery path [26]. Fu et al. [27] examined the seismic response of a bridge pier by pointing out the key factors that influence the effects of repairs. Additionally, as previously mentioned, the restoration function estimates (measured in time units) incorporate delays related to decision-making, financing, and inspections to assess the average recovery time for highway bridge functions. This study examines the relationship between repair times and various damage states through the framework established by Fereshtehnejad and Shafieezadeh [28] for four specific damage states. Generally, as damage severity rises, more time is required to repair the damage and

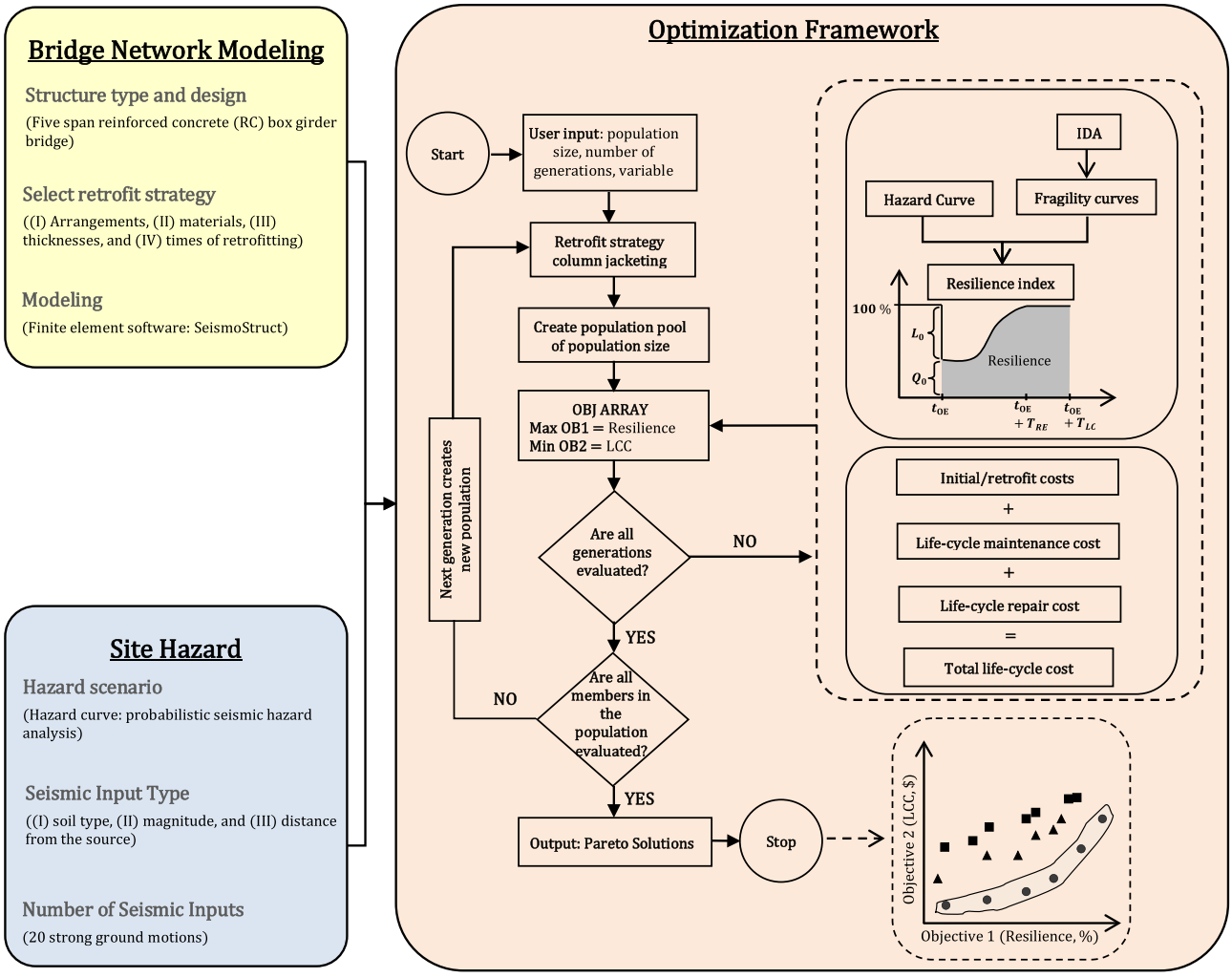

Fig. 1. An overview of the optimization procedure of this study.

Table 1
Required recovery time thresholds for seismic damage states and corresponding statistical data [28].

Damage state (DS_k)	Recovery path	Recovery time (Days)			
		Log-normal mean (Log-normal standard deviation)			
		T_{ins}	T_{mob}	$T_{d\&c}$	T_{rep}
Slight	$T_{ins}+T_{d\&c}+T_{rep}$	4 (3.6)	- (-)	30 (27.4)	0.6 (0.6)
Moderate	$T_{ins}+T_{mob}+T_{d\&c}+T_{rep}$	4 (3.6)	45 (41.0)	40 (36.5)	2.5 (2.7)
Extensive	$T_{ins}+T_{mob}+T_{d\&c}+T_{rep}$	4 (3.6)	45 (41.0)	50 (45.6)	75 (42)
Complete	$T_{ins}+T_{mob}+T_{d\&c}+T_{rep}$	4 (3.6)	45 (41.0)	60 (54.7)	230 (110)

return the structure to its original (or intact) condition. In this context, the respective probabilistic log-normal recovery functions, which indicate the required times, are presented in Table 1. In this table, T_{ins} refers to the time necessary for inspection and assessment, $T_{d\&c}$ indicates the time needed to develop a repair plan, secure bids, and finalize contracts, T_{mob} represents the mobilization time for resources (including materials and teams), while T_{rep} denotes the duration required for actual repairs.

3. Theoretical foundations of fragility curves

Given the unpredictable nature of earthquake occurrences, a probabilistic approach is reasonable to evaluate structures' seismic vulnerability [29]. Therefore, the likelihood of exceeding a predetermined level of performance can be stated based on a specific Intensity Measure (IM). For this purpose, the fragility curves are utilized to demonstrate the probability of reaching each damage state (i.e., slight, moderate, extensive, and complete as the kth damage state; DS_k) for a range of ground motion intensity measure levels. Li [30] developed a probability-based seismic risk and ground motion framework to propose high-precision seismic risk functions and models for structure portfolios, incorporating the influence of ambient temperature on structural fragility that is often ignored.

The appropriate selection of the Engineering Demand Parameter (EDP) and IM is pivotal in developing fragility curves. In this line, Li and Zhong [31] proposed a seismic vulnerability and risk model for bridges that incorporates both instrumental and macroseismic intensity measures. Also, Li and Gardoni [32] introduced an optimized Gaussian distribution model that comprehensively considers the impact of instrument intensity and seismic hazard models on traditional macroseismic intensity. In addition, Li [33] presented an innovative bivariate inten-

Table 2
Threshold of damage state quantities prescribed by HAZUS [25] for the case of initial intact state.

Damage State (DS_k)	Description	Fragility Curve ($\Delta = u_{max}/H$)	
		μ_k	σ_k
Slight	Minor cracking and spalling to the abutment, cracks in shear keys at abutments, minor spalling and cracks at hinges, minor spalling at the column (damage requires no more than cosmetic repair) or minor cracking to the deck.	0.01	0.6
Moderate	Any column experiencing moderate (shear cracks) cracking and spalling (column structurally still sound), moderate movement of the abutment (<2″), extensive cracking and spalling of shear keys, any connection having cracked shear keys or bent bolts, keeper bar failure without unseating, rocker bearing failure or moderate settlement of the approach.	0.025	0.6
Extensive	Any column degrading without collapse – shear failure – (column structurally unsafe), significant residual movement at connections, or major settlement approach, vertical offset of the abutment, differential settlement at connections, shear key failure at abutments.	0.05	0.6
Complete	Any column collapsing and connection losing all bearing support, which may lead to imminent deck collapse, tilting of substructure because of foundation failure.	0.075	0.6

sity measurement method and a hybrid seismic vulnerability quantification approach to evaluate building clusters during two earthquakes in Qinghai Province, resulting in a consistent prediction of economic losses aligned with actual observations. In this respect, various Damage Indices (DIs) with different types of IM such as Peak Ground Acceleration (PGA), Peak Ground Velocity (PGV), Arias Intensity (AI), Spectral acceleration (Sa), and Spectral displacement (Sd) have already been proposed by several studies. Recently, Aristeidou and O'Reilly [34] examined the performance of a novel IM that incorporates ground motion directionality and structure non-linearity.

The damage index is chosen based on piers' maximum relative displacement (or drift), which is usually preferred as the damage index because of its physical sense-making [35,36]. These constant drift limits better serve as a global (system) response quantity [37]. This study considers the maximum drift of the bridge pier and the PGA as the EDP and IM indices because of their practicality, efficiency, and sufficiency in seismic vulnerability assessment, respectively [38–39]. It should be noted that the PGA is used as a suitable IM for large-scale seismic risk reduction plans such as bridge networks to prioritize retrofit programs [40–44]. In a probabilistic seismic vulnerability assessment framework, the conditional probability $P_E(\cdot|\cdot)$ of demand exceeding capacity can be evaluated as follows:

$$P_E\left(D \geq DS_k | IM\right) = \phi\left[\frac{1}{\sigma_k} \ln\left(\frac{EDP}{\mu_k}\right)\right] \tag{4}$$

where the log-normal cumulative distribution function, $\phi[\cdot]$, is used to construct fragility curves according to log-standard deviation (σ_k) and median value (μ_k) for each damage state based on HAZUS [25] (see Table 2). It should be noted that the choice of distribution for fragility curves is critical and often dependent on empirical data characteristics, the nature of the structural response, and specific uncertainties of the seismic environment. The log-normal distribution is frequently selected due to its flexibility and ability to model the multiplicative and skewed nature of parameters affecting damage, offering a realistic framework for assessing seismic fragility compared to simpler models like normal or exponential distributions. In this regard, fragility curves are typically derived from the analytical EDP data predicted by the previously mentioned methods, employing a probabilistic model. The lognormal distribution, defined by two parameters (i.e., log-standard deviation (σ_k) and median value (μ_k)) is the most commonly utilized model in these analyses. It is widely recognized and applied in numerous parametric analytical fragility studies [1,2,5,6,8,9,11,16–19,25,28,37,45–48].

4. Life-cycle cost analysis (LCCA)

The total life-cycle cost incurred costs, C_{TOT}, in an infrastructure throughout its service lifetime generally includes (I) initial construction costs C_{IN}, (II) total life-cycle maintenance costs C_M, and (III) total life-cycle repair costs resulting from hazard events like earthquakes C_{RP}. In this regard, it is essential to calculate the expected value of these costs, considering future uncertainties. The Net Present Value (NPV) is used to compare and calculate the discounted values of these costs in different years as:

$$\bar{C}_{TOT,NPV} = \bar{C}_{IN} + \bar{C}_{M,NPV} + \bar{C}_{RP,NPV} \tag{5}$$

in which $\bar{C}_{TOT,NPV}$, $\bar{C}_{IN}$, $\bar{C}_{M,NPV}$, and $\bar{C}_{RP,NPV}$ represent the discounted NPV of the total life-cycle cost incurred costs, initial construction costs, total life-cycle maintenance costs, and total life-cycle repair costs, respectively. For an existing infrastructure, $\bar{C}_{IN}$ will be equal to zero in the LCC calculations. However, if there are plans to upgrade the infrastructure, $\bar{C}_{IN}$ equals the upgrade costs. In addition, routine maintenance intervention is frequently undertaken to ensure that infrastructure performs optimally. To determine the annual NPV of the total life-cycle maintenance costs, the following relationship can be used:

$$\bar{C}_{M,NPV} = \sum_{t=1}^{T_{LC}-1} \gamma^t \times \bar{C}_{M,t} \tag{6}$$

where $\bar{C}_{M,NPV}$ represents the total expected life-cycle maintenance costs at a specific year t, while T_{LC} indicates the expected service lifetime of the infrastructure. In addition, the annual discount factor is represented by $\gamma = \frac{1}{1+r}$, and r denotes the discount rate. In a similar approach to how $\bar{C}_{M,NPV}$ is evaluated, the net present value of total expected life-cycle repair costs for future years can be determined as:

$$\bar{C}_{RP,NPV} = \sum_{t=0}^{T_{LC}-1} \gamma^t \times \bar{C}_{RP,t} \tag{7}$$

in which the term $\bar{C}_{RP,t}$ represents the total expected life-cycle repair costs within the time span $[t, t+1]$, which can be formulated as a function of the potential damage conditions. By employing the total probability rule (also known as the law of total probability), this term can be derived using as follows:

$$\bar{C}_{RP,t} = \sum_{k=1}^{N_{LS}} \bar{C}_{rp}\left(LS_k\right) \times P_E\left(LS_k, [t, t+1]\right) \tag{8}$$

where N_{LS} stands for the total number of structural limit states, and $\bar{C}_{rp}(LS_k)$ represents the total expected life-cycle repair costs when the structure is in a limit state k. The term $P_E(LS_k, [t, t+1])$ indicates the likelihood of the structure being in a limit state k within the time span $[t, t+1]$. Moreover, $\bar{C}_{rp}(LS_k).P_E(LS_k, [t, t+1])$ is commonly referred to as the risk cost being at the kth structural limit state. The interpretation of the right side of Eq. (8) is that it represents the difference in cumulative risk cost between experiencing the kth structural limit state over the period $[0, t+1]$ and that of the interval $[0, t]$, as:

Table 3
The ratio of the median of damage states for calculating fragility curves, when the structure is intact, to the median of damage states, when the structure is not initially in the intact state [45].

Damage state in fragility curve for initial intact limit state	Damage state in fragility curve for initial below limit state					
	Slight			Moderate		Extensive
	Moderate					
Moderate	1.25	Extensive		Extensive		
Extensive		1.25	Complete	1.5	Complete	Complete
Complete			1.25		1.5	2

$$\bar{C}_{RP,t} = \sum_{k=1}^{N_{LS}} \left\{ \bar{C}_{rp}\left(LS_k\right) \times P_E\left(LS_k, [0, t+1]\right) - \bar{C}_{rp}\left(LS_k\right) \times P_E\left(LS_k, [0, t]\right) \right\} \tag{9}$$

In terms of mathematics, it is probable that an unspecified number of earthquake events (denoted as n) may occur over a specified time span. Again, by employing the total probability rule for the cumulative risk cost and n events within the time span $[0, t]$ for each limit state k, this cost can be calculated as follows:

$$\bar{C}_{rp}\left(LS_k\right).P_E\left(LS_k, [0, t]\right) = \sum_{n=1}^{\infty} P_{nt}(n, t)\left(\sum_{j=1}^{n} \left\{ \bar{C}_{rp}\left(LS_k\right).P_E\left(LS_k^j n, t\right) \right\} \right) \tag{10}$$

where $P_{nt}(n, t)$ shows the likelihood of independent n events occurring within the time interval $[0, t]$. This probability can be derived using the Poisson distribution function, where υ represents the rate of hazard occurrence. In this line, $P_E(LS_k^j n, t)$ indicates the likelihood of the system experiencing the kth structural limit state during the jth hazardous event. In addition, $P_E(LS_k^j n, t)$ quantifies the probability of incomplete repairs, allowing for the assessment of cumulative damage.

To determine the risk cost of Eq. (10), it is necessary to compute $P_E(LS_k)$ as the probability of exceeding a damage state for the understudy system. In this regard, in Section 3, different damage states (i.e., slight, moderate, extensive, and complete) are categorized as the 1st, 2nd, 3rd, and 4th seismic damage states. Subsequently, fragility curves are developed by utilizing the maximum drift of the bridge pier derived from structural analysis by utilizing the median and log-standard deviation parameters extracted from Tables 2 and 3 [28,45]. Therefore, the probability of being in a limit state k between two consecutive damage states can be calculated by:

$$P_E\left(LS_k\right) = P_E\left(DS_k\right) - P_E\left(DS_{k+1}\right) \tag{11}$$

The condition of the infrastructure after a hazardous event is influenced by various factors, including the type of the hazard, its severity, and the infrastructure's damage state before the event. In this line, when a hazardous event causes damage to a structure, a repair program is carried out to restore the system to its intact (or original) state. However, suppose another hazardous event happens before these repairs are finished. In that case, the expected damage condition is likely to be more severe than the damage that would have occurred if the structure had remained intact. For this scenario, it can be logically inferred that the damage condition is identical to before repairs began. Like the concept of $P_E(LS_k^j|n, t)$, term $P(DS_k^j n, t)$ can be calculated for a specific hazard type as follows:

$$P_E\left(DS_k^j n, t\right) = \sum_{k'=1}^{N_{LS}} \sum_{RS} P_E\left(DS_k^j\left[RS_{k'}, LS^{j-1}{}_{k'}\right], IM, n, t\right). P\left(\left[RS_{k'} LS^{j-1}{}_{k'}, IM, n, t\right]\right).P_E\left(\left[LS^{j-1}{}_{k'} n, t\right]\right).P(IM) \tag{12}$$

in which $P(IM)$ is the likelihood of the particular hazard intensity and can be determined by considering a hazard curve depicting the frequency of hazards exceeding a certain intensity measure; $\frac{1}{\upsilon}.|\Delta\lambda(IM)|$. The term $RS_{k'}$ in Eq. (12) refers to the structure repair status after the $(j-1)$th hazardous event, indicating if it has been fully repaired ($RS_{k'} = 1$) or not ($RS_{k'} = 0$). By applying the Bayes rule, one can write:

$$P\left(\left[RS_{k'} = 0 LS^{j-1}{}_{k'}, n, t\right]\right) = \frac{P\left(\left[RS_{k'} = 0, n, t LS^{j-1}{}_{k'}\right]\right)}{P_{nt}(n, t)} \tag{13}$$

When the structure is in the limit state k' after the $(j-1)$th hazardous event, the repair status is considered incomplete if the time interval between the $(j-1)$th and jth hazards is shorter than the required time to carry out the repairs for the limit state k', denoted as $\tau_{k'}$. In this case, the system is assumed to remain in the limit state k', resembling its condition after the $(j-1)$th hazardous event. Considering that there are n hazard events occurring within the time interval $[0, t]$, the probability of the unfinished repair action at the jth event can be expressed as $P((t_j - t_{j-1}) < \tau_{k'}, \{(j-2), [0, t_{j-1}]\}, \{0, [t_{j-1}, t_j]\}, \{(n-j),\ [t_j, t]\})$. This term indicates that the time interval between the $(j-1)$th and the jth hazards should be shorter than the demanded time for repair actions ($t_j - t_{j-1} < \tau_{k'}$). By applying the total probability rule, this concept can be formulated as follows:

$$\begin{aligned} P\left((t_j - t_{j-1}) < \tau_{k'}, \left\{(j-2), \left[0, t_{j-1}\right]\right\}, \left\{0, \left[t_{j-1}, t_j\right]\right\}, \left\{(n-j),\ \left[t_j, t\right]\right\}\right) &= P\left(\left[RS_{k'} = 0, n, t LS^{j-1}{}_{k'}\right]\right) \\ &= \int_0^t \int_{t_{j-1}}^{\min\{t_{j-1}+\tau_{k'}, t\}} P\left((j-2), \left[0,\ t_{j-1}\right]\right).P\left(0, \left[t_{j-1},\ t_j\right]\right). \\ &\quad P\left((n-j),\ \left[t_j,\ t\right]\right).\upsilon^2.dt_j.dt_{j-1} \end{aligned} \tag{14}$$

where $P((j-2), [0, t_{j-1}])$ is the Poisson probabilities of $(j-2)$ events, which occur during $[0, t_{j-1}]$ (or $\{(j-2), [0, t_{j-1}]\}$). Similarly, $P(0, [t_{j-1}, t_j])$ is the Poisson probabilities that no hazardous event should occur during $[t_{j-1}, t_j]$ (or $\{0, [t_{j-1}, t_j]\}$). Also, $P((n-j),\ [t_j,\ t])$ is the Poisson probabilities of $(n-j)$ hazards should take place following the jth hazard during $[t_j, t]$ (or $\{(n-j),\ [t_j, t]\}$).

The fragility curve is a key parameter in the LCC computational framework, as portrayed in Section 3. In addition, it is assumed that the structure is undamaged or that the process of repair had been completed before the jth hazardous event. Alternatively, if neither of these conditions were met (i.e., intact state), it would be necessary to establish new thresholds for damage states to compute fragility curves. In this regard, the ratios of median damage states for undamaged and damaged structures can be derived from Raghunandan et al. [45], as shown in Table 3. Fig. 2 presents an overall flowchart outlining the infrastructure LCC assessment framework encountering potential risks.

5. Modeling an illustrative bridge network

In general, infrastructures include simple to complicated systems. The presented life-cycle cost and resilience optimization framework can be applied to different types of infrastructure. To implement this methodology, the first step involves selecting the specific infrastructure and identifying potential natural hazards as hazard curves. Fragility curves are then constructed in accordance with structure type and site characteristics. Afterward, life-cycle cost and resilience can be determined using the presented formulation. These fundamental steps are iterated by considering different retrofit strategies, and the desired objectives (namely, the life-cycle cost, the resilience, and the cost of retrofit)

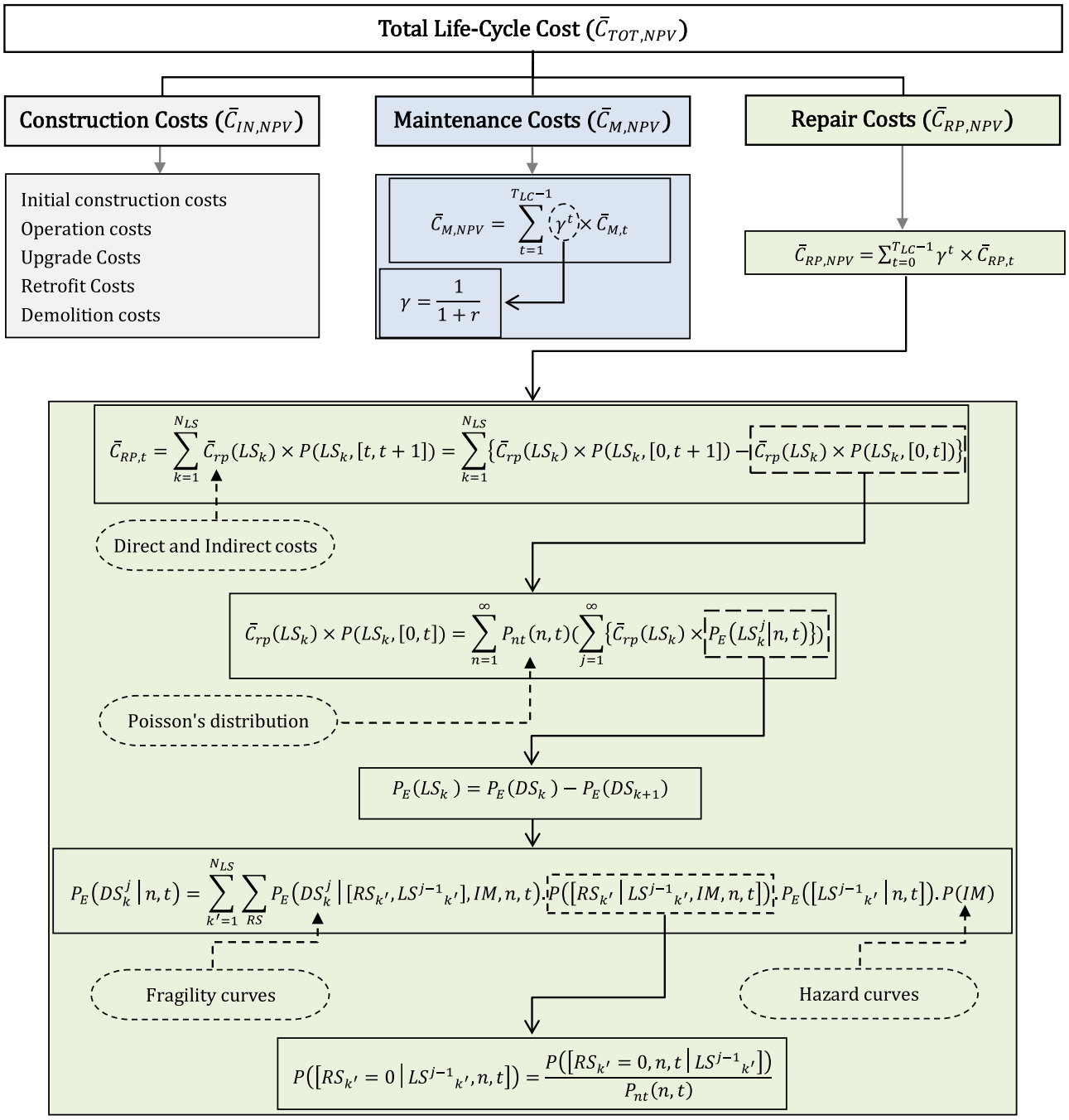

Fig. 2. Flowchart for calculating the LCC assessment of infrastructure systems.

are assessed to find the best strategies. An illustrative and simple bridge network model is used to explain the steps involved in implementing the multi-objective optimization framework outlined in this study. In this respect, a detailed discussion of all the steps involved in the proposed optimization framework is explicitly provided for under-study infrastructure.

5.1. Bridge network

The proposed multi-objective optimization framework has been applied to an illustrative bridge network as a case study infrastructure. However, this framework can be adjusted, extended, and used for the entire highway infrastructure of a region or a country. For this purpose, the illustrated transportation network in Fig. 3 is employed, which includes 11 bridges and 28 lanes. The network's bridge type is the Multi-Span Continuous Concrete Box Girder (MSC–CBG) bridge. The decision-maker can employ the LCC-R assessment framework to prioritize the mitigation measures, including retrofitting and/or monitoring of critical assets, optimization of recovery strategies and disaster preparedness, insurance of the infrastructure against natural disasters, and planning for the extension of the network.

5.2. Bridge structure

The bridge model used in this study is based on the design presented by Sultan and Kawashima [49]. This bridge is considered an RC box girder bridge with three lanes and five spans, including three 53.3 m interior spans and two 39.6 m exterior spans. Fig. 4 presents further de-

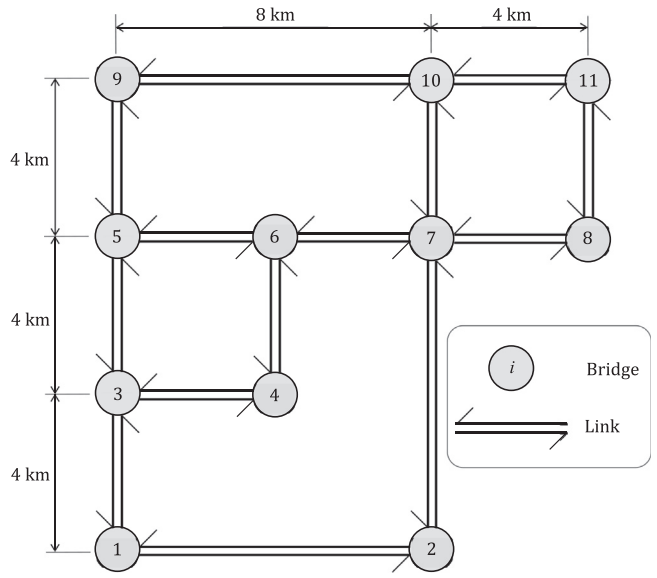

Fig. 3. Schematic transportation network topology and bridges considered in this study.

tails of the bridge structure modeled in Finite Element (FE) SeismoStruct software [50].

This research uses NTH-IDAs to evaluate the under-study structure's response. The structural elements are defined using a three-dimensional inelastic force-based frame element to correctly model material nonlinearity. To accurately calculate the damage distribution in the elements, the SeismoStruct requires the definition of cross-section behavior [50]. For this purpose, the cross-sections are partitioned into the predetermined number of fibers (generally 200), where each fiber represents the uniaxial stress-strain relationship. Therefore, the stress-strain conditions of the beam-column elements are subsequently determined by integrating the nonlinear uniaxial stress-strain behavior of each individual fiber (Refer to Appendix A for the validation and verification of the FE modeling conducted with SeismoStruct software [50]).

The concrete material is represented by utilizing the uniaxial nonlinear variable confinement model developed by Madas and Elnashai [51] that follows the constitutive relationship proposed by Mander et al. [52] along with cyclic rules proposed by Martinez-Rueda and Elnashai [53]. For steel bar material, FE modeling employs a uniaxial steel model initially introduced by Yassin [54], incorporating the isotropic hardening rules suggested by Filippou et al. [55]. In this line, the current implementation is based on the work carried out by Monti et al. [56]. Also, an additional memory rule is utilized to improve the numerical stability and accuracy under transient seismic loading, according to Fragiadakis et al. [57]. Regarding the material characteristics of the steel jacket, a uniaxial stress-strain model with kinematic strain hardening is simulated, as presented in Table 4. The modeling of the Fiber Reinforced Polymer (FRP) material involves using a simplified uniaxial trilinear FRP model, which assumes no compressive resistance [58]. CFRP and GFRP are represented as TU27C-QuakeWrap and VU27G-QuakeWrap, respectively, in SeismoStruct [50]. The model allows for varying numbers of FRP layers. Both composite materials incorporate high-strength unidirectional fabrics, with material properties sourced from the product data sheets of QuakeWrap Inc. (refer to Table 4) [50]. In cases where the RC pier is wrapped with steel/FRP jackets, the concrete cover is considered concrete confined by the steel/FRP jacket, whereas the concrete core is considered concrete confined by the FRP and the transverse bars. For considering the effect of FRP wrapping on concrete confinement properties, the model developed by Ferracuti and Savoia [59] is utilized, which incorporates the confining effect of the jacketing materials using the model developed by Spoelstra and Monti [60]. This model is based on the constitutive relationship and cyclic rules for compression and tension states, as presented by Yankelevsky and Reinhardt [61], respectively. Also, the abutments are regarded according to the guidelines outlined in Choi [62]. The abutment model incorporates an additional passive soil effect in the longitudinal direction based on Maroney et al. [63]. Based on Caltrans recommendations [64], each pile's effective stiffness is set at 7 kN/mm. To address the impact between the abutment and the deck, a 'bilinear gap' impact element [65] is utilized. This element is modeled using non-linear springs with parameters K and Δ_{gap}. In this analysis, the maximum deformation or penetration Δ_{gap} is assumed to be 25.4 mm between adjacent decks and 40 mm between the end of the deck and the back wall of the abutment. The stiffness parameter K is derived using the model proposed by Muthukumar and DesRoches [65].

For bridge retrofitting, the RC piers are wrapped with three different materials (i.e., steel, CFRP, and GFRP) in four different thicknesses (T1 to T4). In this line, steel jackets are used in thicknesses of 9.53, 12.7, 19.05, and 25.40 mm. Also, the RC piers are jacketed with CFRP and GFRP, using 2, 4, 7, and 10 plies; the thickness of each ply is 1.24 and 1.27 mm, respectively. Moreover, eight arrangements (A1 to A8) for the bridge piers are considered for the retrofit design, as depicted in Fig. 5.

5.3. Strong ground motion selection and structural analysis

This study employs the recognized NTH-IDA method to produce fragility curves for calculating seismic resilience curves/surfaces and the LCC. A critical factor in the nonlinear dynamic analysis of structures is the selection of a sufficient number of appropriate records, as the results of the analyses are heavily reliant on the input ground motion [66]. Shome and Cornel [67] suggested that using 10 to 20 Strong Ground Motions (SGMs) can reflect satisfactory estimates of how a structure responds under certain conditions. Therefore, this study utilizes 20 SGMs gathered from the PEER database [68]. Table 5 presents the selected strong ground motions data corresponding to earthquake magnitudes of approximately $5.5 \sim 7.5$ and the typical soil classification (i.e., $360 \leq V_{S30} \leq 760$ m/s). It should be noted that in this research, both horizontal components (i.e., the L and T components, or x and y directions) of each earthquake are applied simultaneously to the under-study bridge, and the vertical component is ignored [69]. Therefore, the maximum structural response is determined using the triangle law of vector addition based on the time history of responses in both directions simultaneously. In this line, Fig. 6(a) displays the acceleration response spectra of 20 SGMs, assuming a damping ratio of 5 %. It is essential to mention that every considered SGM is divided into ten levels, ranging from PGA = 0.1 g to 1 g, with each increment of PGA = 0.1 g. In addition, the hazard curves are probabilistically assumed for the bridge's location for the PGA as the IM, using an online application developed by the United States Geological Survey (USGS) [70]. To investigate the effect of seismic hazards on the LCC and resilience parameters, it is assumed that the under-study bridge network area is classified into three seismic zones: high, medium, and low. In this line, these three seismic intensity levels, as hazard curves, are assumed to be 0.5 g, 0.35 g, and 0.2 g, corresponding to the PGA for a 475-year return period (with a 10 % probability of exceedance in 50 years). It should be noted that high, medium, and low seismic zones include 3, 4, and 4 bridges, respectively. Furthermore, the resilience index in the multi-objective optimization process is determined by an earthquake recurrence interval of 475 years based on the Probabilistic Seismic Hazard Analysis (PSHA) conducted at the research site, as shown in Fig. 6(b).

5.4. Cost terms

In this study, various cost terms are taken into account and added together as $\bar{C}_{rp}(LS_k)$ in Eq. (8) to calculate the LCC. A brief overview of each of these cost terms is provided below.

In this regard, the composite fabrics cost \$31.65/m^2 for GFRP and \$105.92/m^2 for CFRP plies. In addition, the steel jacket has a unit cost of

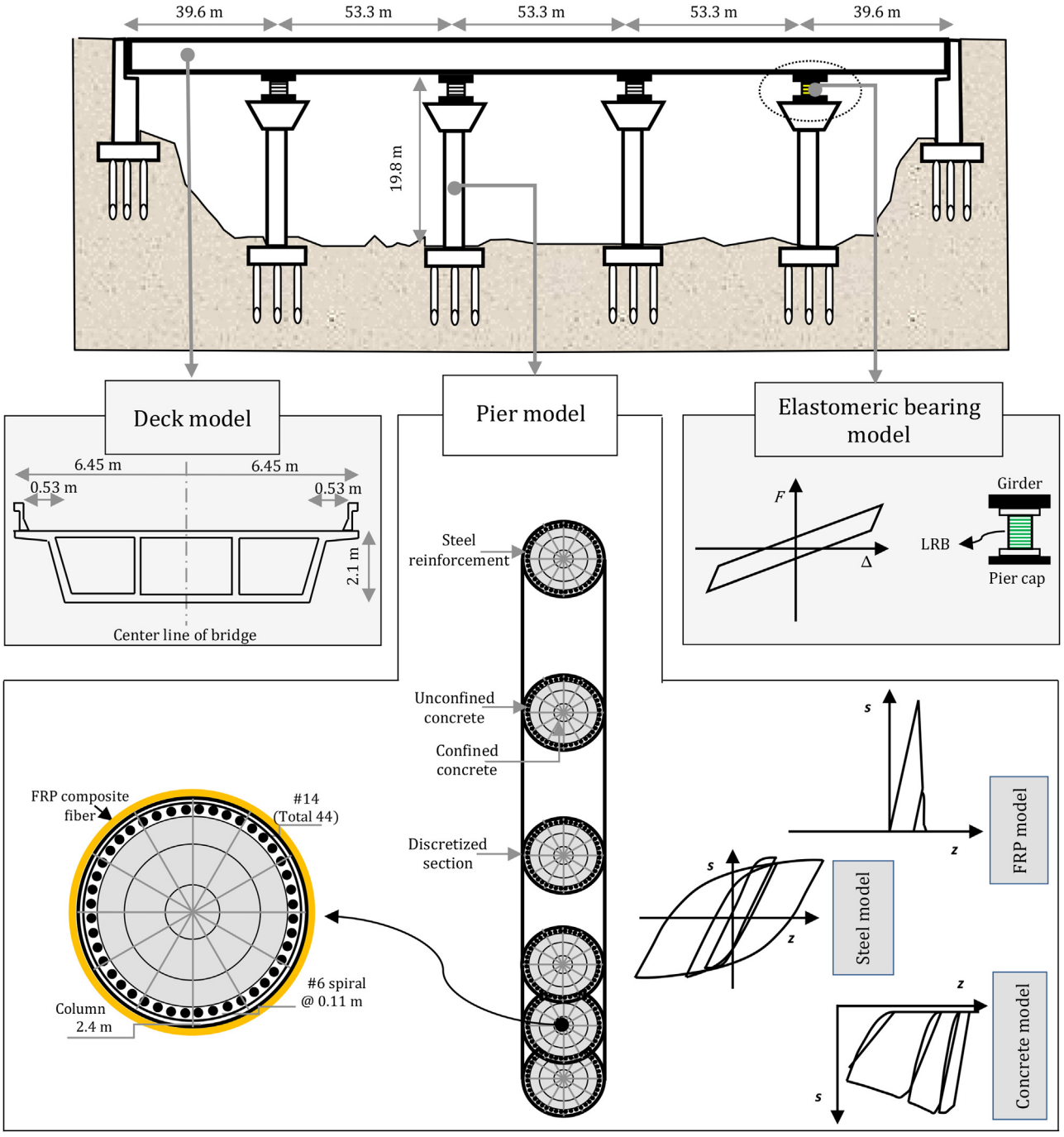

Fig. 4. Finite element model specifications of considered bridge in SeismoStruct software.

$500/ton. As per Caltrans [71] construction data, the average replacement cost of an RC box girder bridge is approximately $1833/m^2. For bridge annual maintenance costs, it can be assumed that 0.5 % of the total replacement cost applies for each year.

In the field of structural loss estimation, several research studies have been carried out to minimize this cost term. In this context, Calvi et al. [72] developed formulations to quickly calculate the average expected annual loss, considering both direct and indirect losses, based on a few straightforward parameters. The framework proposed by Calvi et al. [72] enables the practical use of loss-based methodologies in seismic design and can be applied to new designs and assessment scenarios. Also, Abarca et al. [73] developed a method for assessing indirect losses resulting from disruptions in road networks, mainly focusing on evaluating the travel delays experienced by users following a bridge collapse as an indicator of indirect losses. Abarca et al. [73] demonstrated that their simplified measure yields reliable estimates of bridge importance compared to more detailed calculations, thereby improving our understanding of how road network disruptions affect resilience.

As emphasized earlier, the community experiences direct and indirect losses following each hazardous event because of incurred damage to infrastructure. Consequently, a more comprehensive assessment of these expenses yields a more dependable life-cycle cost estimation. In this study, the following categories of costs are taken into account: (1) repair costs associated with structural damage, (2) environmental damage costs, (3) costs associated with delay time, vehicle operation, and

Table 4
Material properties used in the finite element analysis.

Material	Material model in SeismoStruct	Mechanical property	Value
Concrete	Mander et al. nonlinear concrete model (con_ma)	Compressive strength (MPa)	35
		Tensile strength (MPa)	3.5
		Modulus of elasticity (MPa)	27,850
		Strain at peak stress	0.002
		Specific weight (kN/m^3)	24
Steel (bar)	Menegotto-Pinto steel model (stl_mp)	Modulus of elasticity (GPa)	200.0
		Yield strength (MPa)	400
		Strain hardening	0.005
		Transition curve initial shape	20
		Transition curve shape calibrating coefficient (A1)	18.5
		Transition curve shape calibrating coefficient (A2)	0.15
		Isotropic hardening calibrating coefficient (A3)	0
		Isotropic hardening calibrating coefficient (A4)	1
		Fracture/buckling strain	0.1
		Specific weight (kN/m^3)	78
Steel (jacketing)	Menegotto-Pinto steel model (stl_mp)	Ultimate tensile strength (MPa)	250
Elastomeric bearing	Symmetric bilinear curve (bl_*sym*)	Initial stiffness (kN/mm)	14.78
		Yield force (kN)	37.77
		Post-yield hardening ratio	0.050
CFRP	Trilinear FRP model (frp_tl)	Tensile strength (MPa)	930
		Tensile modulus (GPa)	89.6
		Ultimate elongation (%)	0.98
		Ply thickness (mm)	1.24
		Specific weight (kN/m^3)	18
GFRP	Trilinear FRP model (frp_tl)	Tensile strength (MPa)	587
		Tensile modulus (GPa)	27.4
		Ultimate elongation (%)	2.3
		Ply thickness (mm)	1.27
		Specific weight (kN/m^3)	18

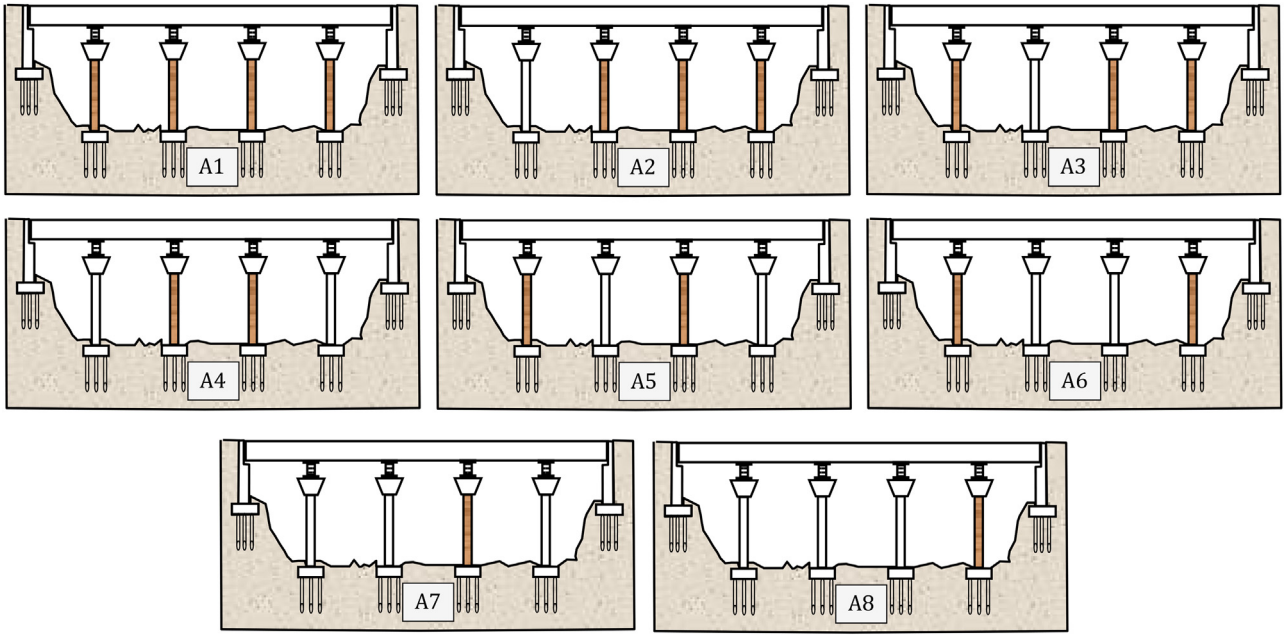

Fig. 5. Various arrangements used for bridge pier retrofitting configurations.

excess gas emissions for users, (4) costs associated with human casualties, and (5) costs associated with economic losses.

5.4.1. Agency repair costs

The repair costs incurred by the agency can be determined by multiplying the replacement cost by a factor r_k for each limit state according to HAZUS [25]. Additionally, Caltrans [71] states that the total life-cycle repair cost should include two additional costs: (1) contingency costs and (2) mobilization costs. These two costs should be added to calculate the total life-cycle repair costs. The contingency costs are estimated to be 20 % of the bridge repair costs, while the mobilization costs are estimated to be 10 %.

5.4.2. Environmental damage costs

As mentioned, the bridge network repair process leads to traffic interruption and delays. Consequently, there is a potential for increased air pollution, energy consumption, and global warming [74]. This incurred cost can be calculated as:

$$C_E\left(LS_k\right) = C_{Env} \times \min\left(\tau_k,\ 1/v\right) \times \left(En_{Vij}^{D/R} - En_{Vij}^{O}\right) \tag{15}$$

where En_{Vij}^{O} and $En_{Vij}^{D/R}$ represent the carbon dioxide emission value at speeds of V_{ij}^{O} and $V_{ij}^{D/R}$, respectively. Based on Gallivan et al. [75], the two mentioned speeds refer to the average velocity of vehicles passing the route ij before and after a hazard event. In addition, the unit en-

Table 5
Strong ground motion records.

Record No.	Earthquake	Year	Station Name	Magnitude	R rupture (km)	PGA (g)	Focal Mechanism
1	Chichi Taiwan	1999	CHY080	7.62	2.69	0.953	Reverse oblique
2	Northridge	1994	Sylmar - Converter Sta East	6.69	5.19	0.963	Reverse
3	Kobe Japan	1995	Nishi-Akashi	6.9	7.08	0.498	Strike-slip
4	Erzincan Turkey	1992	Erzincan	6.69	4.38	0.488	Strike-slip
5	Loma Prieta	1989	Corralitos	6.93	3.85	0.662	Reverse oblique
6	Helena Montana	1935	Carroll College	6	2.86	0.196	Strike-slip
7	Nahanni Canada	1985	Site 1	6.76	9.6	1.019	Reverse
8	Corinth Greece	1981	Corinth	6.6	10.27	0.272	Normal oblique
9	Norcia Italy	1979	Cascia	5.9	4.64	0.213	Normal
10	Izmir Turkey	1977	Izmir	5.3	3.21	0.41	Normal
11	Northern California	1941	Ferndale City Hall	6.4	44.52	0.115	Strike-slip
12	San Fernando	1971	Fairmont Dam	6.61	25.58	0.111	Reverse
13	Tabas Iran	1978	Boshrooyeh	7.35	24.07	0.106	Reverse
14	Imperial Valley	1979	Calipatria Fire Station	6.53	23.17	0.129	Strike-slip
15	Friuli Italy	1976	Codroipo	6.5	33.32	0.091	Reverse
16	Victoria Mexico	1980	SAHOP Casa Flores	6.33	39.1	0.1	Strike-slip
17	Irpinia Italy	1980	Bovino	6.9	44.62	0.046	Normal
18	Coalinga	1983	Cantua Creek School	6.36	23.78	0.288	Reverse
19	Kern County	1952	Taft Lincoln School	7.36	38.42	0.18	Reverse
20	Northern California	1954	Ferndale City Hall	6.5	26.72	0.203	Strike-slip

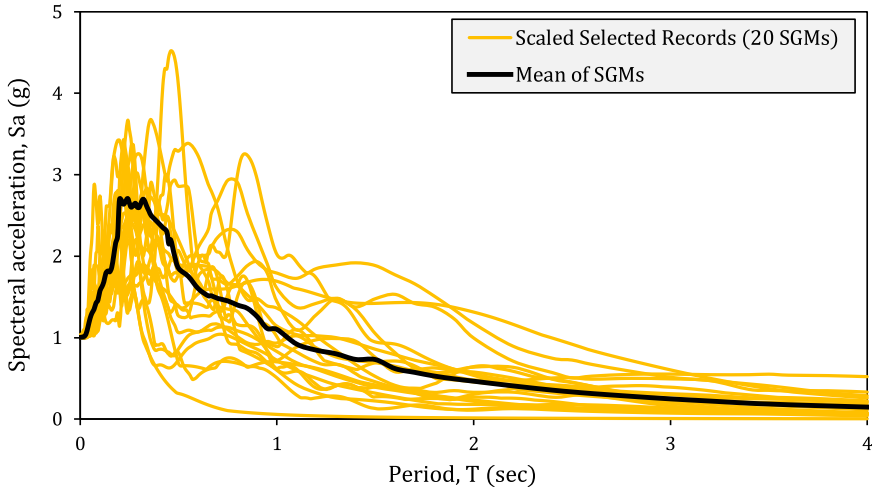

(a)

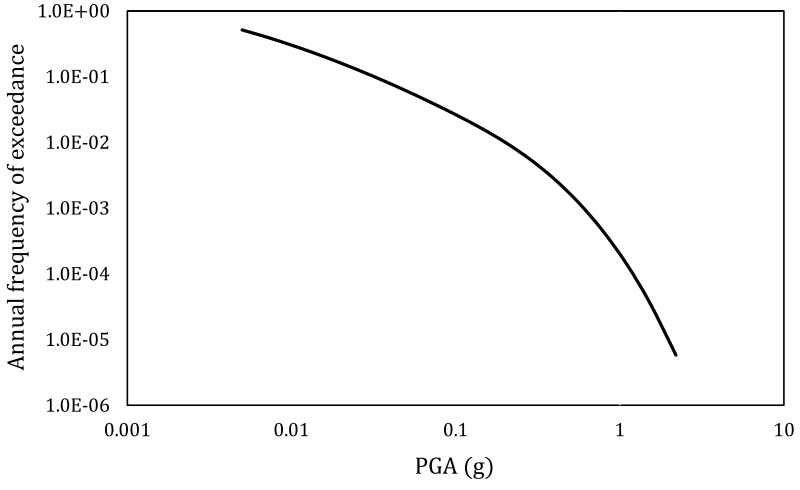

(b)

Fig. 6. Site characteristics for (a) spectral acceleration versus time period for considered earthquake records and (b) hazard curves for the case study bridge system in high seismicity area.

Table 6
Default relationships for estimating population distribution and casualty rates for bridges based on HAZUS [25].

Distribution of people in census tract (Commuting)			
Occupancy	2:00 a.m.	2:00 p.m.	5:00 p.m.
Commuting in cars	0.005(POP)	(PRFIL)0.05(POP)	(PRFIL)[0.05(POP)+1.0(COMM)]
Commuting using other modes		0.50(1-PRFIL)0.05(POP)	0.05(1-PRFIL) [0.05(POP)+1.0(COMM)]

Note 1: The casualty rate is considered 17 %, 20 %, 37 %, and 7 % for casualty severity levels 1–4.
Note 2: POP is the census tract population taken from census data, and COMM is the number of people commuting inferred from census data.
Note 3: PRFIL is a factor representing the proportion of commuters using automobiles, inferred from profile of the community (0.60 for dense urban, 0.80 for less dense urban or suburban, and 0.85 for rural).

vironmental damage costs term C_{Env} is $33.49/ton of carbon dioxide emission, as stated by Kendall et al. [76].

5.4.3. User costs of imposed delay, vehicle operation, and excess emission

Closing the bridge site, either partially or entirely, is often inevitable to ensure the safety of workers/users while repairing damaged elements. As a result, users experience delays, overworked vehicles, and the emission of excess gases due to traffic disruptions and increases in fuel consumption, such as hydrocarbons, carbon monoxide, and nitrous oxide [77]. For example, Abarca et al. [78] introduced a seismic risk methodology, which has been applied to a case study involving 617 bridges in the Italian province of Salerno by analyzing the Average Annual Loss (AAL), taking into account the median expenses related to car fuel efficiency, fuel prices, and hourly wage rates relevant to the Salerno region. These factors contribute to the user cost, denoted as $C_U(LS_k)$, which can be determined based on the damage repair costs for the under-study bridge as follows [79]:

$$PC_U(LS_k) = \min(\tau_k,\ 1/\upsilon) \times \left(t_{ij}^{D/R} - t_{ij}^{O}\right) \times \left[(AADT - AADTT) \times \rho_C + AADTT \times \rho_T\right] \quad (16)$$

in which $\min(\tau_k,\ 1/\upsilon)$ indicates traffic disruptions expected time, which is calculated as the minimum of the required repair time for the kth limit state (τ_k, as indicated in Table 1) and the expected time difference between successive hazardous events. For the under-study bridge network, the Annual Average Daily Traffic ($AADT$) and the Annual Average Daily Truck Traffic ($AADTT$) values for route ij are set at 77,000 and 7392, respectively [77]. Also, t_{ij}^{O} and $t_{ij}^{D/R}$ are correspond to the time taken to pass the route ij without or with partial/complete closures, as determined by Bocchini and Frangopol [80]. Lastly, ρ_C and ρ_T are $21.79 per hour and $58.83 per hour, respectively [81].

5.4.4. Cost of human casualties

The possible outcome of a damaged bridge network is human casualties, which include both injuries and deaths. The costs of human casualties, $C_H(LS_k)$, can be determined based on the kth limit state as:

$$C_H(LS_k) = \sum_{t=1}^{4} C_{SLt} \times CR_k^{SLt} \times NPAR \quad (17)$$

where C_{SLt} is the cost of human casualties for a particular severity level t. The casualty rate for a severity level t and the kth limit state is denoted by CR_k^{SLt}, and $NPAR$ indicates the total number of people at risk. These terms for the under-study bridge are adopted based on the research of Porter et al. [82], HAZUS [25], and Caltrans [83], respectively. In this line, a report released by the California Highway Patrol [84] encompasses various elements of a significant bridge failure. This document thoroughly details most of the facts surrounding the structural collapse. The majority of injuries and deaths occurred on the lower northbound deck due to the upper deck collapsing onto it. Additionally, a considerable number of injuries and fatalities were recorded among drivers on the upper southbound deck. A smaller number of casualties also happened to individuals on the surface streets next to the collapsed structure. The model attempts to estimate casualties to people either on or under bridges that experience complete damage. The number of people on or under bridges and the bridge casualty rates are calculated in Table 6.

5.4.5. Cost of economic losses

Businesses near the transportation network will experience adverse effects from traffic disruptions caused by bridge damage following earthquake events and the bridge network repair process. In this respect, Kliesen and Mill [85] suggested that the cost of economic losses can be estimated as twice the user costs of imposed delay, vehicle operation, and excess emission.

6. Optimal retrofit strategies

Optimization is a systematic process of finding the most optimal solution or set of solutions for problems with either single- or multi-objectives, respectively. These optimization problems require either maximizing or minimizing the values of objective functions. This research investigates various optimization objectives using NSGA-II through Single-Objective Optimization (SOO) and Multi-Objective Optimization (MOO). As a result, the optimization problems are divided into three sections: (I) the SOO, which focuses solely on minimizing the life-cycle cost; (II) the MOO-1, which aims to maximize resilience and minimize the cost of retrofit; and (III) the MOO-2, which aims to maximize resilience and minimize life-cycle cost. In this regard, Table 7 demonstrates the fundamental concept of the optimization problem in this study.

Table 7
The main steps of the multi-objective optimization framework using the NSGA-II.

Initialize
User input: population size ($\boldsymbol{N_p}$), random initial population ($\boldsymbol{P_t} \subset \boldsymbol{S}$), number of generations $\boldsymbol{t_{max}}$, variable limit
Retrofit design: Arrangements ($\boldsymbol{a}$: Various plans used for retrofitting configurations) **&**
Materials ($\boldsymbol{m}$: Steel, CFRP, GFRP) **&**
Jacket thickness: ($\boldsymbol{j}$: Steel jacketing: 9.53, 12.7, 19.05, 25.40mm
CFRP jacketing: 2, 4, 7, 10 PLY (each ply=1.24 mm)
GFRP jacketing: 2, 4, 7, 10 PLY (each ply=1.27 mm)) **&**
Time of retrofitting: (t_i: Various time of retrofitting used for LCC)
Start
While ($t < t_{max}$) **do**
Generate offspring ($\boldsymbol{Q_t}$)
Mutate on $\boldsymbol{Q_t}$
Set $\boldsymbol{R_t} = \boldsymbol{P_t} \cup \boldsymbol{Q_t}$
Evaluate objective functions:
Resilience index ($\boldsymbol{a}, \boldsymbol{m}, \boldsymbol{j}$)
Life-cycle cost ($\boldsymbol{a}, \boldsymbol{m}, \boldsymbol{j}, \boldsymbol{t_i}$)
(or **Cost of retrofit** ($\boldsymbol{a}, \boldsymbol{m}, \boldsymbol{j}$))
Apply non-dominated sorting on $\boldsymbol{R_t}$:
Maximize : **Resilience Index**
Minimize : **Life-cycle cost** (or **Cost of retrofit**)
Next generation:
Best of $\boldsymbol{R_t}$ population
End while
Return the best set of solutions (Pareto Front)
End

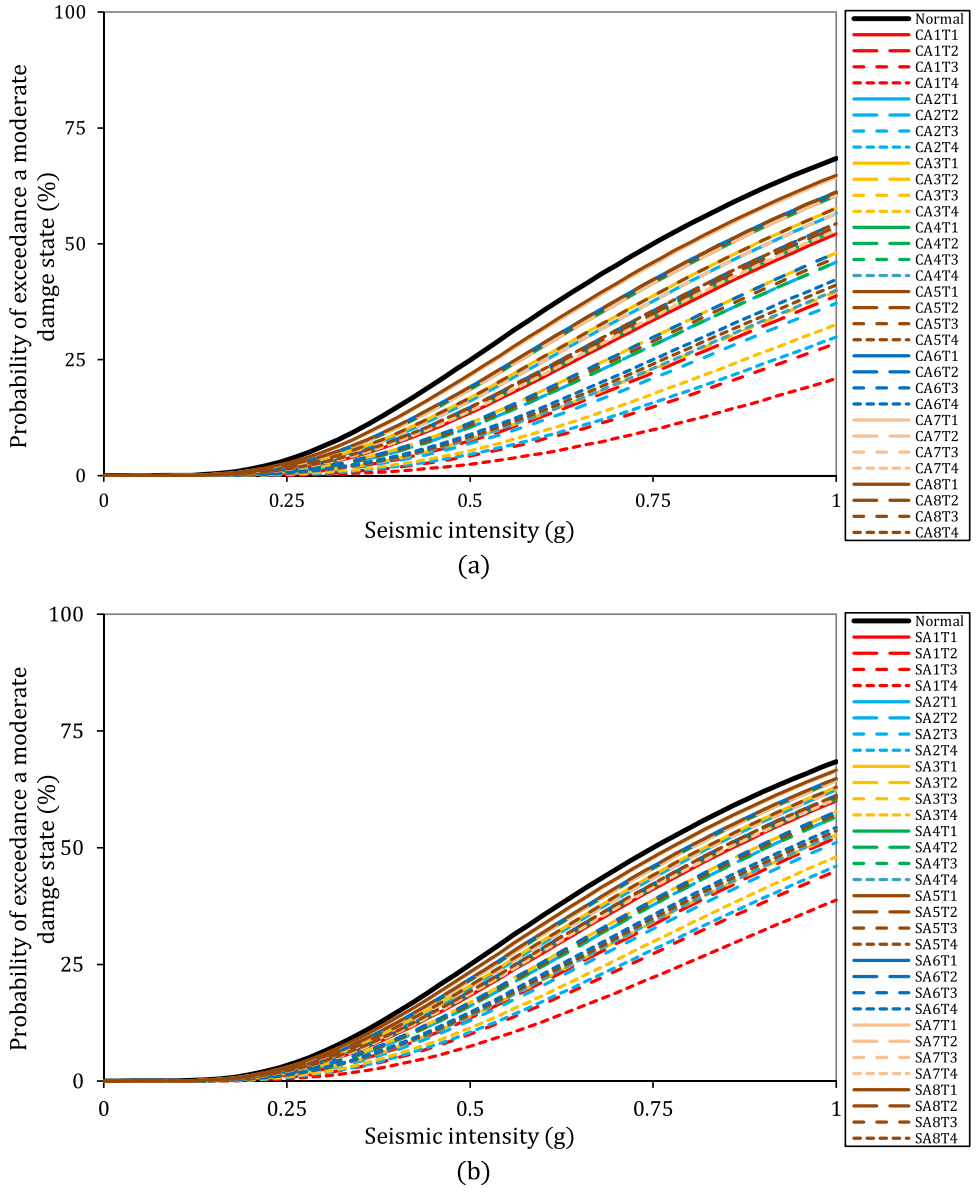

Fig. 7. Seismic vulnerability assessment in the form of (a) fragility curves for CFRP jacketing, (b) steel jacketing at the moderate damage state, (c) resilience curves for CFRP jacketing right after an event, and (d) upper and lower bounds of resilience surfaces for GFRP strategies.

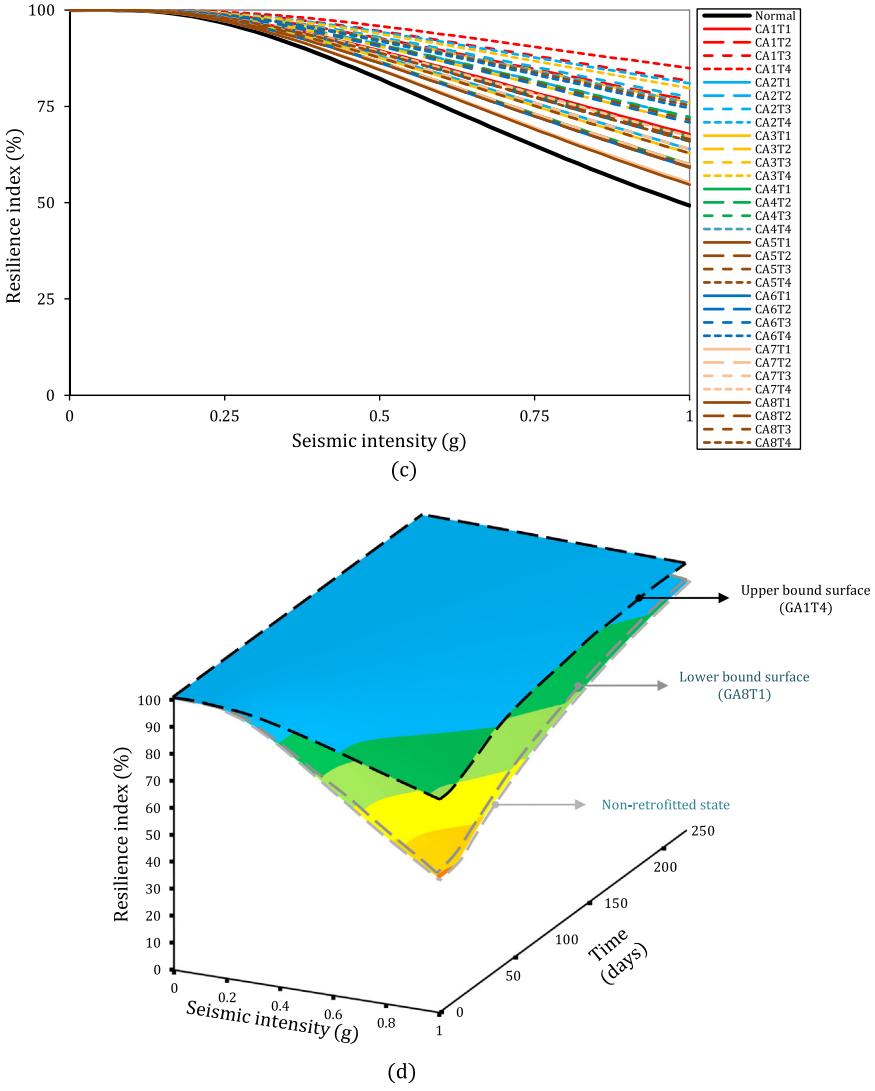

Fig. 7. Continued

6.1. *Fragility and resilience curves*

The fragility curves are a valuable tool for estimating the seismic vulnerability of a system/component, such as a bridge/pier. It is the first step in assessing the resilience and life-cycle cost. In this process, the probabilities of pre-defined damage states are determined by assuming a log-normal distribution function for each retrofit design result obtained from the IDAs. The fragility curve is generated according to the average structural response subjected to seismic SGMs, as shown in Fig. 7(a - b). The results show that the difference in fragility values among the various retrofit designs primarily depends on structural parameters (including different materials, arrangements, and thicknesses) and site-specific seismic hazard parameters like seismic intensity level. This difference becomes more pronounced, particularly for non-retrofitted structures, as the input seismic intensity and damage state increase from slight to complete. Also, jacketing bridge piers with additional layers reduces the discussed difference due to the structure experiencing less non-linear behavior. As shown in Fig. 7, using CFRP jacketing has the greatest impact on reducing vulnerability, as indicated by the fragility curves. For example, despite having similar thicknesses of SA1T2 (12.7 mm) and CA1T4 (12.4 mm) in their retrofit strategies (Fig. 5), their fragility values differ significantly. In this line, under the same conditions at PGA = 0.6 g, the likelihood of experiencing slight damage is approximately 59 % for SA1T2 and 35 % for CA1T4.

In the subsequent step, resilience can be determined by utilizing fragility curves and recovery functions, as outlined and clarified in Section 2. The resilience index is deemed a more understandable and logical parameter for decision-makers than fragility curves. These resilience curves can serve as a reference point for program progression in short-, medium-, and long-term planning. To assess the resilience index, various retrofit designs are evaluated in the form of curves and surfaces, as depicted in Fig. 7(c-d). The resilience curve illustrates the seismic resilience value immediately following an earthquake event of varying intensities. In contrast, the resilience surface displays how the infrastructure recuperates to its original condition through repairs. It is discernible that appropriate retrofit designs mitigate the infrastructure's susceptibility to destructive factors, such as seismic input intensity, resulting in greater reliability and predictability.

6.2. *Total life-cycle cost analysis*

6.2.1. *Total life-cycle maintenance cost*

As previously mentioned, one of the main objectives of this study is to minimize the life-cycle cost of existing infrastructure, including the costs of retrofit, repair, and maintenance throughout its service lifetime. The total life-cycle maintenance cost is calculated per the bridge's value (as formulated in Section 4), including its initial construction cost and the cost of retrofitting if necessary. Fig. 8 illustrates the total life-cycle

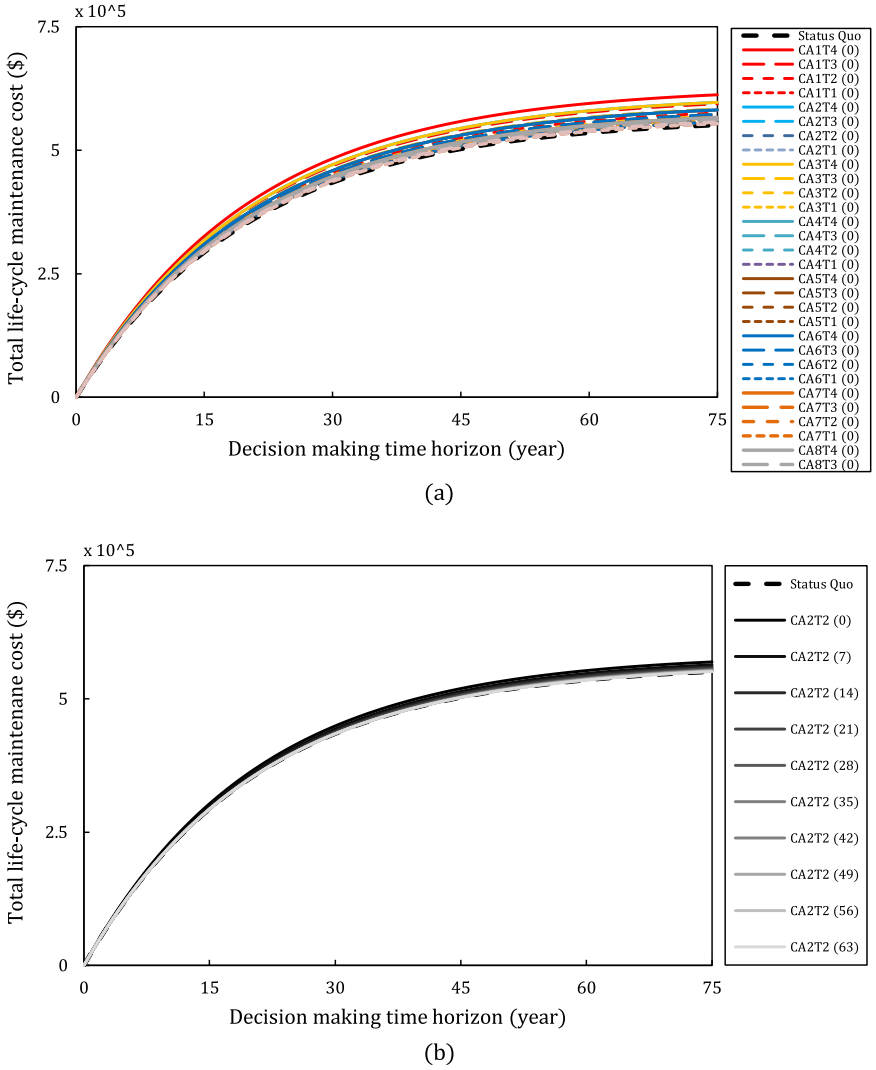

Fig. 8. The total life-cycle maintenance cost for (a) CFRP jacketing, (b) CA2T2 retrofit arrangement at different times of retrofitting, (c) R/N ratio for CFRP jacketing, and (d) R/N ratio mean values for different jacking materials .

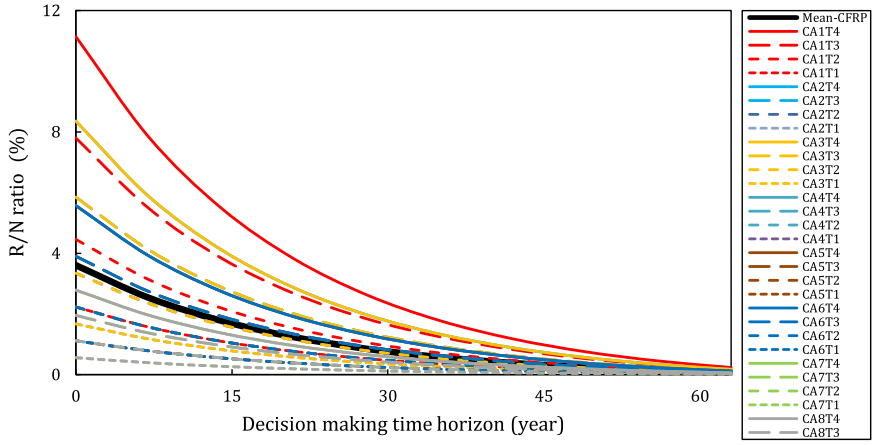

(c)

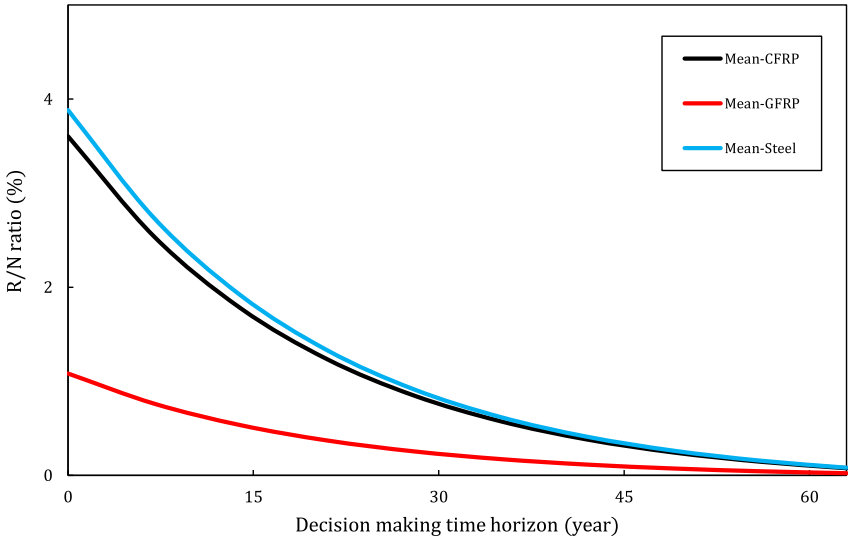

(d)

Fig. 8. Continued

maintenance cost for the chosen retrofit design, considering all relevant cost assumptions. It can be observed from Fig. 8(a) that the increase in this cost is dependent on the amount of material (T1 to T4) and pier jacketing (A1 to A8) used compared to the non-retrofitted bridge. Additionally, the impact of retrofitting at various time intervals is analyzed concerning this cost by assuming intervals of 7 years ranging from 0 to 70 years in Fig. 8(b).

The results indicate that the total life-cycle maintenance cost increases at different rates for various retrofit strategies, as shown in Fig. 8(a – b). To analyze this point more comprehensively, the R/N ratio is considered, R denotes the total life-cycle maintenance cost of retrofitted structures and N represents the cost for non-retrofitted structures (Fig. 8(c)). Furthermore, Fig. 8(d) presents the average R/N ratio of different retrofit strategies. Based on the results, retrofitting raises the total life-cycle maintenance cost by approximately 3 % on average.

6.2.2. *Total life-cycle repair cost*

The most crucial term in estimating the total life-cycle cost is the repair cost. The effects of seismic hazard risks, including the different site seismicity and the structure's vulnerability, can be calculated using this cost term. Therefore, the total life-cycle repair cost is a crucial parameter in LCC to determine the best retrofit strategy for an infrastructure. This cost term includes direct losses from structural damage and indirect losses from various factors, as explained in Section 5.4. The total life-cycle repair cost is evaluated within the framework for different retrofit strategies and seismic zones, as depicted in Fig. 9.

Fig. 9(a) demonstrates that the total life-cycle repair cost can vary in compliance with two factors, namely (I) hazard curves and (II) fragility curves. Hazard curves reflect site hazard characteristics such as seismicity state, while fragility curves represent the structure's vulnerability in terms of dynamic structural properties. These factors are inherently involved in the LCC computational formulation for estimating the total life-cycle repair, ultimately leading to the superiority of certain retrofit strategies over others. For example, consider the A4 to A6 retrofit designs, which have an equal number of retrofitted piers (Fig. 5) and, therefore, result in equal total life-cycle maintenance costs, exhibit differences in their total life-cycle repair costs. Hence, the A4 retrofit design further decreases the total life-cycle repair cost by enhancing structural resilience against seismic input. This is due to the jacketing of more central piers compared to the two similar retrofit designs. Moreover, the timing of retrofitting can significantly influence the increase or decrease in this cost term (Fig. 9(b)). The results show that the timing of retrofitting greatly influences the reduction in total life-cycle repair cost when it does in the early years. This effect diminishes as the retrofit

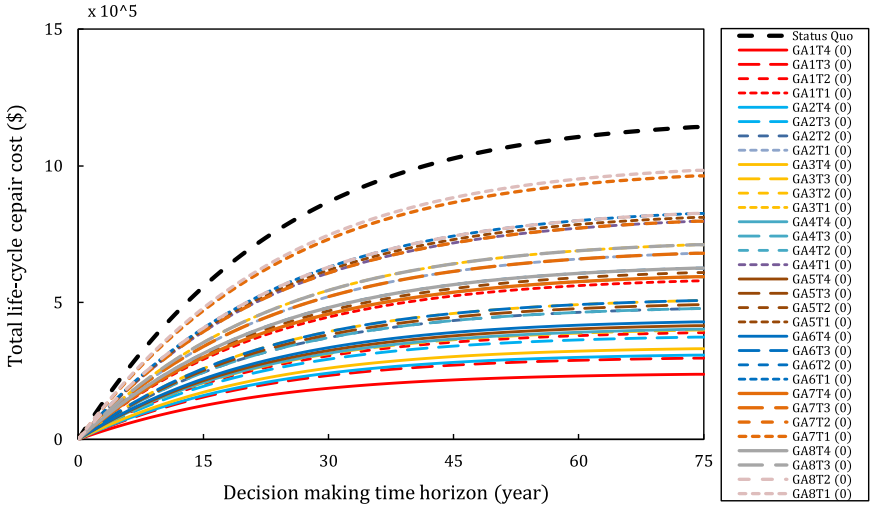

(a)

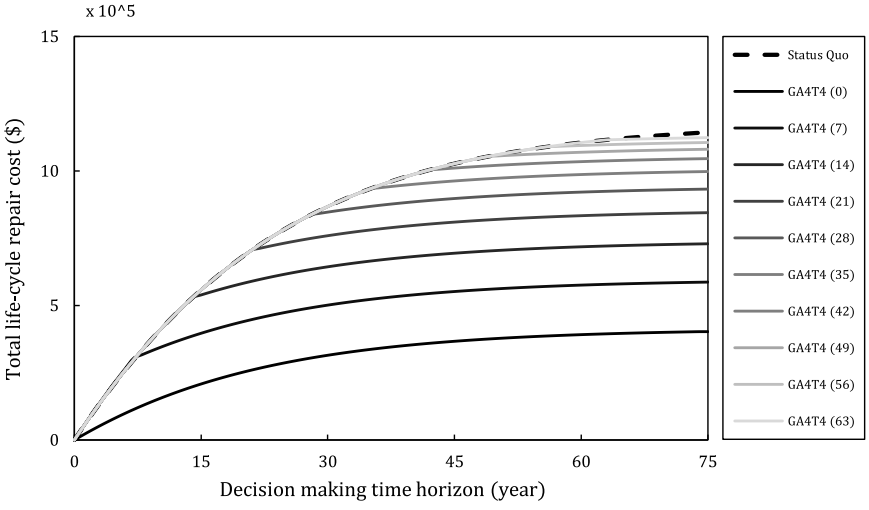

(b)

Fig. 9. The total life-cycle repair cost for (a) GFRP jacketing, (b) GA4T4 strategy at different times of retrofitting, (c) retrofit efficiency for GFRP, and (d) retrofit efficiency mean values for different jacking materials in high seismicity area .

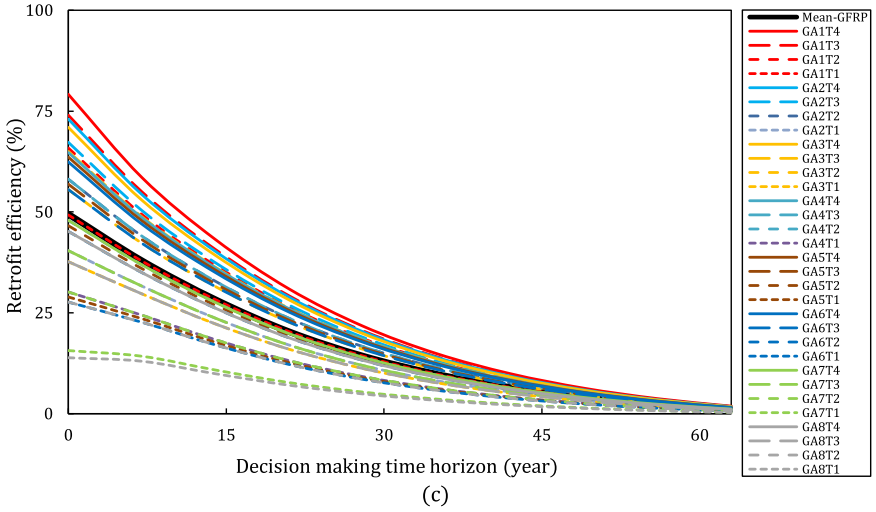

(c)

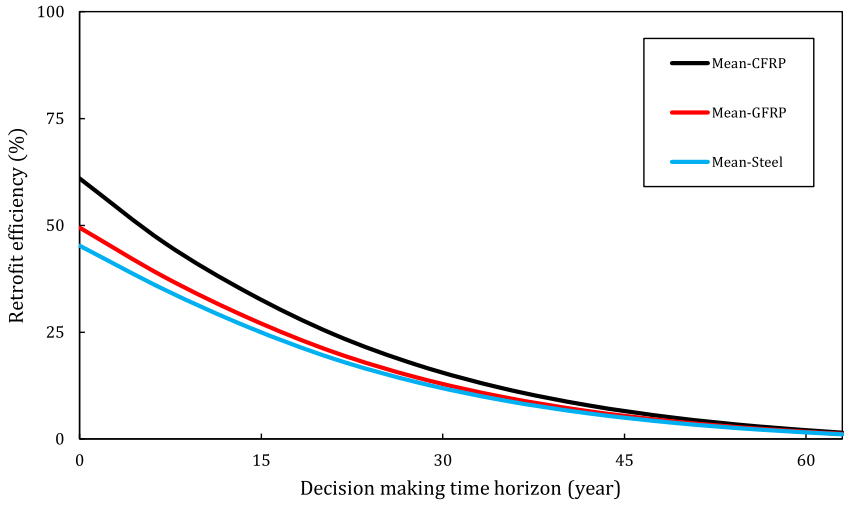

(d)

Fig. 9. Continued

program is postponed. This observation aligns with the PGA values of the hazard curve in different years and their corresponding fragility values. To investigate this aspect, the Retrofit Efficiency ratio ($RE(\%)$) is defined as the ratio of "useful output" to "total input" for the seismic resilience index as follows:

$$RE(\%) = \frac{\text{Useful output}}{\text{Total output}} \times 100\% \tag{18}$$

where the useful output denotes the amount of the reduction in the total life-cycle repair cost due to retrofitting compared to the non-retrofitted bridge. In addition, the total input indicates the total life-cycle repair cost of the non-retrofitted bridge. Fig. 9(c) plots the RE for different GFRP jacketing retrofit strategies. For example, the RE ratios for the GA1T2 (0) and GA1T2 (21) retrofit strategies for a bridge in high seismic zones are about 66 % and 26 %, respectively. This indicates the impact of retrofitting timing, as well as different arrangements, thicknesses, and materials, in reducing the total life-cycle repair cost compared to the non-retrofitted bridge. Fig. 9(d) represents the mean RE ratio of the total life-cycle repair cost for various retrofit strategies and under-study bridge, which is located in high seismic zones.

It is essential to mention that the RE ratio for the total life-cycle repair cost for bridges in regions with high seismicity is approximately similar and slightly higher in percentage compared to regions with medium and low seismicity, and this value is not significant in terms of percentage. However, the RE ratio is relatively the same for regions with different seismicity; the important point is the numerical difference between the total life-cycle repair costs of retrofitted and non-retrofitted structures, which manifests itself more prominently in areas with higher seismicity, particularly in terms of the LCC.

6.2.3. *Total life-cycle cost*

To determine the total life-cycle cost, the cost of retrofit must be included in the total costs of maintenance and repair over the lifespan using the Heaviside step function. Each retrofit strategy is evaluated, and its life-cycle cost is calculated (Fig. 10). The results demonstrate that implementing any retrofit design does not always reduce or optimize the total life-cycle cost compared to the status quo (or non-retrofitted case). For instance, the life-cycle cost for a retrofit design like SA1T2 (0) is lower than that of the non-retrofitted structure, whereas SA1T4(0) with more jacketing material leads to an increase in life-cycle cost and is considered uneconomical according to the LCC criterion in regions with moderate seismicity (Fig. 10(a)). On the other hand, SA1T2 (0) is also more effective in reducing life-cycle cost than SA8T1 (0), with fewer jacketing material criterion in regions with moderate seismicity. Therefore, when choosing the best retrofit designs, the cost of retrofit and the total life-cycle repair cost are more significant factors to consider than the total life-cycle maintenance cost, especially if the total life-cycle cost is the sole criterion. The timing of retrofitting is another essential fac-

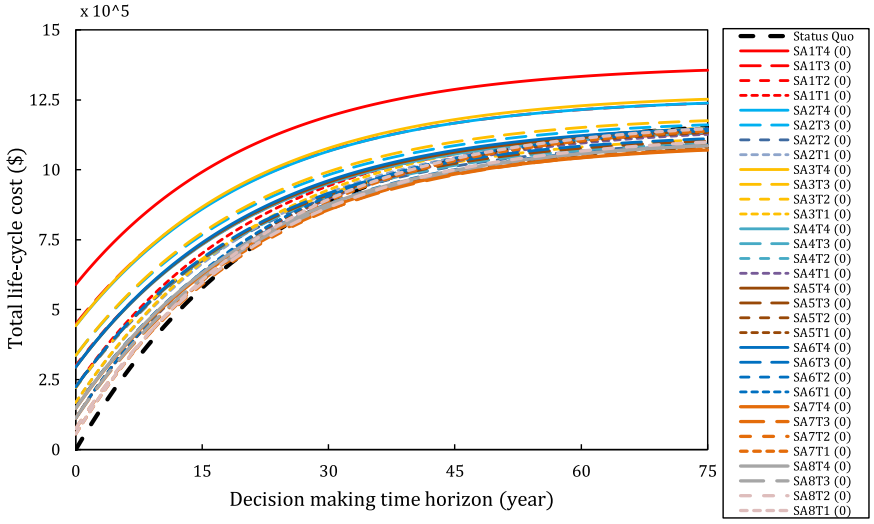

(a)

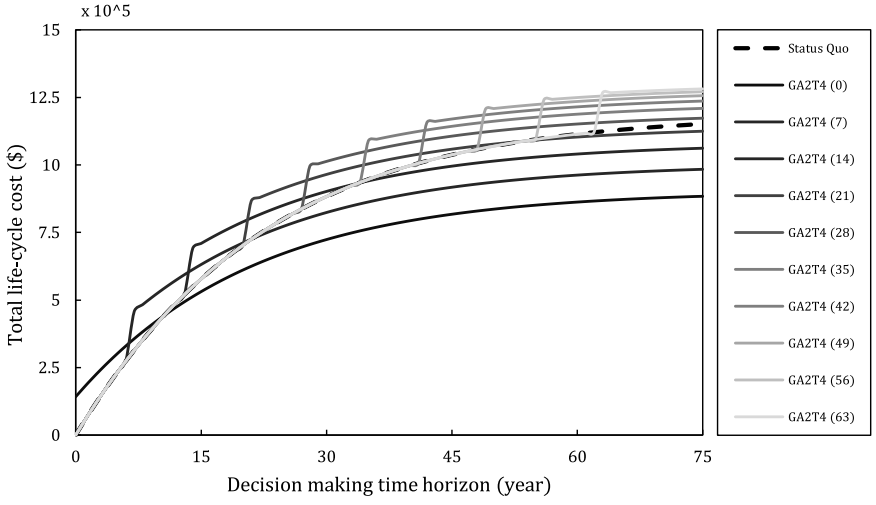

(b)

Fig. 10. The total life-cycle cost for (a) steel jacketing, (b) GA2T4 strategy at different times of retrofitting, (c) retrofit efficiency for GFRP in medium seismicity area, and (d) retrofit efficiency mean values for different seismicity and jacking materials .

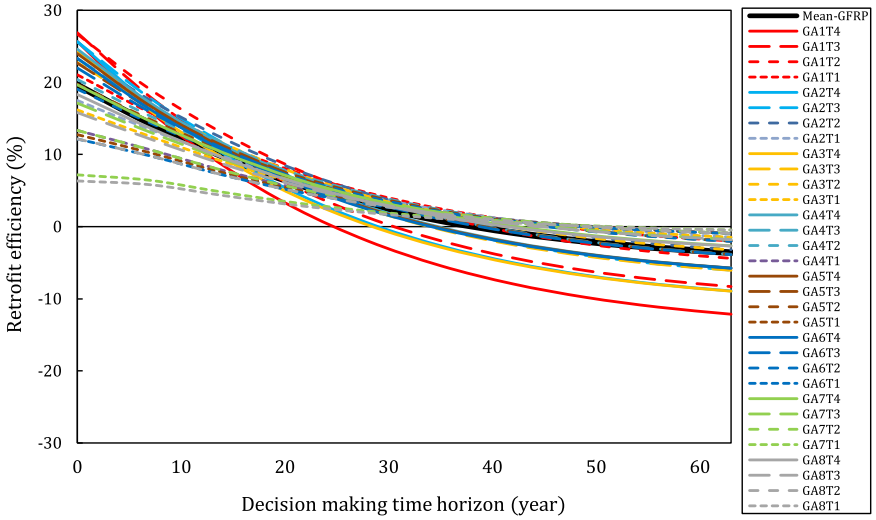

(c)

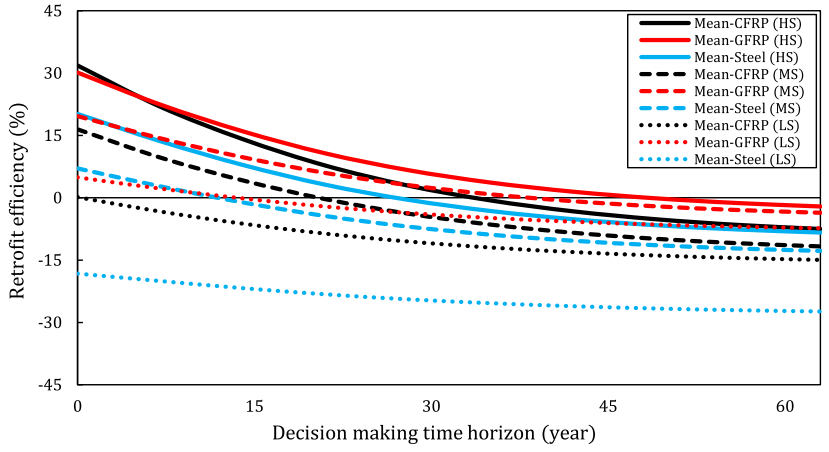

(d)

Fig. 10. Continued

tor, particularly in large-scale projects with budget planning calendars. The impact of retrofitting measures in different years is illustrated in Fig. 10(b).

As evident from Fig. 10(a-b), retrofitting time and other variables involved in retrofit design exert an indisputable impact on the increase or reduction of the total life-cycle cost. In this regard, if a retrofit design is planned to be implemented in the early years (as a retrofit strategy), the LCC is generally reduced. Conversely, if a retrofit strategy is implemented in later years, its effectiveness in lowering the LCC decreases and may even increase the LCC compared to the status quo. To further analyze this section's results, the RE ratio is employed for the LCC. In this case, a positive RE ratio suggests a decrease in the LCC, whereas a negative RE ratio signifies an increase in the LCC (Fig. 10(c-d)). Also, it can be seen that retrofitting designs in areas with higher seismicity are more effective in reducing LCC.

6.2.4. Single-objective optimization

This section implements the optimization framework to illustrative bridge network (see Section 5) using NSGA-II through single-objective optimization, focusing solely on minimizing the life-cycle cost. In this line, a series of assumptions are needed for each large-scale retrofit program to solve the optimization problem for the bridge network (for example, see [40–44]). In this study, the following assumptions are considered for optimization purposes in the under-study bridge network:

- It is assumed that all bridges can be retrofitted within 21 years;
- The bridge retrofit program can be divided into three selected seven-year periods, including (I) the first seven-year (0–7th year) plan, (II) the second seven-year (8–14th year) plan, and (III) the third seven-year (15–21th) plan;
- Two boundary states can be considered for the retrofitting of all bridges, including (1) the lower bound, where all bridges are retrofitted in the first seven-year (hereafter, 11BL), and (2) the upper bound, where all bridges are retrofitted in the third seven-year (hereafter, 11BU).

As discussed, the LCC optimization of the bridge network is considered single-objective optimization, as shown in Fig. 11. It should be noted that 11BL and 11BU indicate the lower and upper bound of retrofit optimization based on the LCC, respectively. In the 11BL strategy, the bridges in the region with high seismicity follow the CA1T2 (0), while the bridges in the region with low and medium seismicity include the GA1T2 (0) retrofit strategy. Also, in the 11BU strategy, the bridges in the region with high seismicity follow the GA1T2 (14). In contrast, the bridges in the region with low and medium seismicity include the GA1T2 (14) and GA1T1 (14) retrofit strategies, respectively. In addition, another strategy called 4–4–3B is considered for the bridge network retrofit strategy. In the 4–4–3B retrofit strategy, four bridges are retrofitted in the first seven-year includes three bridges in the re-

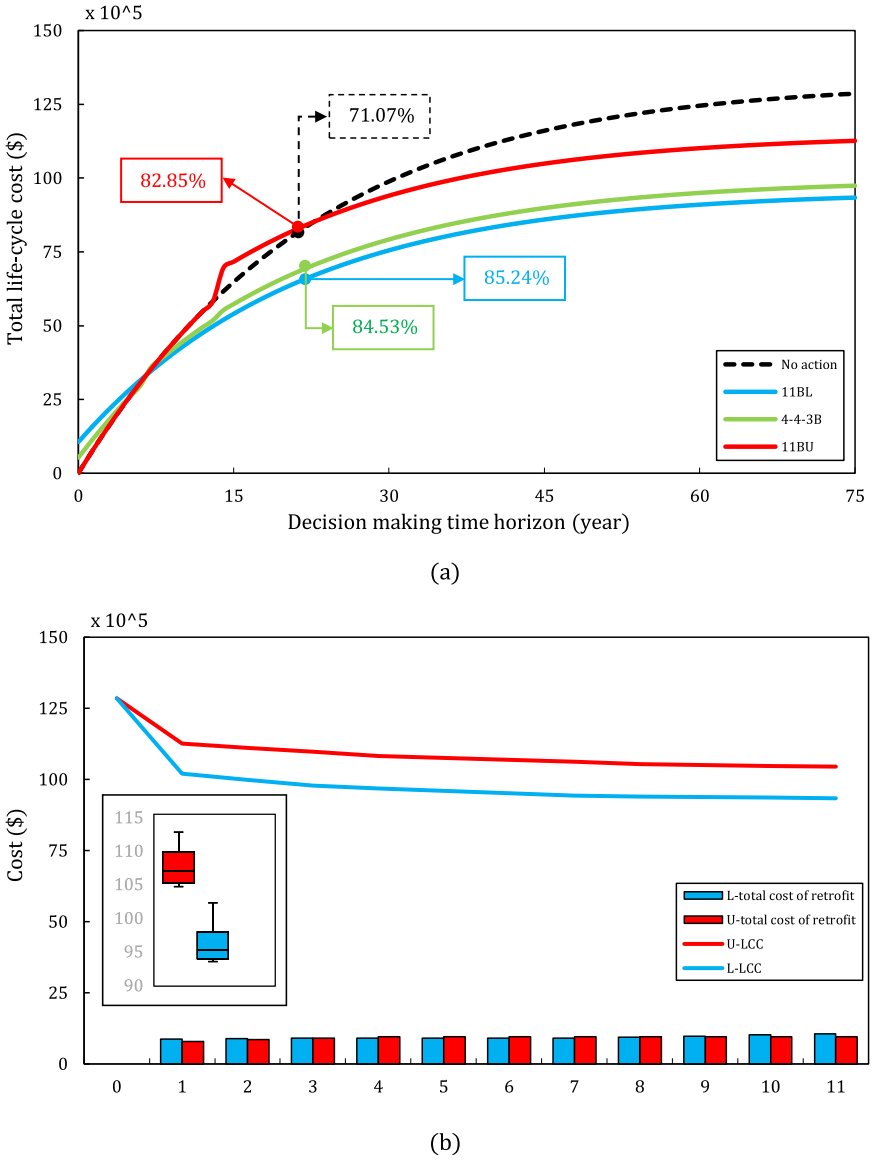

Fig. 11. Comparison between different bridge network retrofit strategies based on the bridge network life-cycle costs and their (a) resilience index, and (b) cost of retrofit.

gion with high seismicity (with CA1T2 (0)) and one bridge in the region with medium seismicity (with strategy GA1T2 (0)). In the second seven years, four bridges are retrofitted, including three bridges in the region with moderate seismicity (with strategy GA1T2 (7)) and one bridge in the region with low seismicity (with strategy GA1T1 (7)). Finally, three bridges are retrofitted in the third seven years and three bridges are in the region with low seismicity (with GA1T1 strategy (14)).

The results of Fig. 11(a) show that the 4–4–3B retrofit strategy is closer to the 11BL retrofit strategy, and the reason for this is the importance of retrofitting bridges in the region with high seismicity due to the high RE of its life-cycle cost. As a result, it is recommended that if there are budget or time limitations for retrofitting all bridges in a transportation network, priority should be given to more vulnerable bridges located in areas with high seismicity. Also, a sub-comparison between the resilience indices of the bridge network is presented for different retrofit strategies at the end of the retrofitting operation (i.e., the third seven-year period) in Fig. 11(a). In this line, the 11BL retrofit strategy has the highest network resilience index because the retrofit strategies based on the optimal LCC in the first year mainly include design with a high ability for earthquake resistance. These retrofit designs include high-resistant materials with more thickness, resulting in increased resilience. However, the resilience index decreases with the later implementation of retrofitting measures. Similarly, a comparison can be made between the lower and upper bounds of retrofit optimization based on the LCC and their cost of retrofit, as shown in Fig. 11(b).

In Fig. 11(b), the horizontal axis indicates the number of bridges that will be retrofitted in the nearest year. Also, the vertical axis indicates the cost (i.e., the LCC for lines and the cost of retrofit for bars). For example, the number 11 on the horizontal axis represents eleven bridges retrofitted as lower bound (blue color) and the upper bound (red color). In this regard, the Box & Whisker charts have been used to compare better the distribution of different retrofitting options within the LCC lower and upper bound. The Box & Whisker charts are often used to describe the dispersion of data. In this chart, a box represents the distance between the first and third quartiles, and a line inside the box represents the middle (second quartile). The minimum and maximum data values are also shown outside the box (Fig. 11(b)).

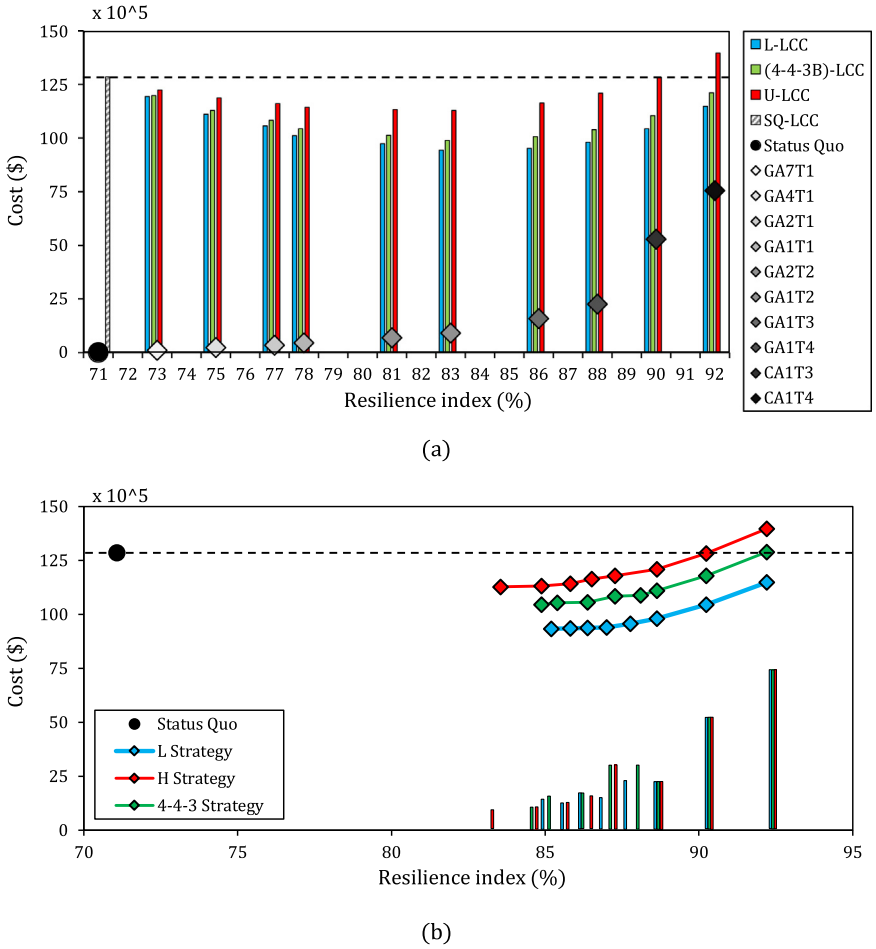

Fig. 12. General trend of the most optimal solutions for (a) the resilience-cost of retrofit, and (b) the resilience-LCC optimization frameworks.

6.2.5. Multi-objective optimization

While the proposed LCC optimization is a suitable and satisfactory framework for single-objective optimization, it lacks a distinct criterion, such as resilience, to effectively demonstrate the level of infrastructure functionality. In this respect, financial and economic factors heavily influence the selection of appropriate retrofit strategies for managing civil infrastructure. Additionally, the resilience index is a reliable measure for evaluating infrastructures' functionality and ability to recover against a hazardous event. To address this issue, two frameworks for multi-objective optimization (the MOO-1 and the MOO-2, as stated in Section 6) are introduced and evaluated for all retrofit strategies being studied within a single-objective optimization framework (i.e., LCC). The resilience–cost of retrofit optimization framework is independent of the timing of retrofitting actions because the two parameters in this optimization framework are independent of time. However, the resilience index depends on the region's seismicity level. Fig. 12(a) shows the set of most optimal retrofit designs for the bridge network based on the resilience–cost of retrofit optimization framework.

In Fig. 12(a), the vertical axis indicates the cost (i.e., the LCC for bars and the cost of retrofit for points). The result of the resilience–cost of retrofit optimization framework can be classified into two distinct parts: (I) retrofit designs that demonstrate a relatively linear relationship between the resilience and the cost of retrofit, which primarily involve jacketing central piers with cheaper yet stronger materials like GFRP instead of steel, and (II) retrofit designs that do not have a linear relationship between these two objectives, which involve jacketing most or all of the bridge piers with thicker materials that are more effective in reducing vulnerability like CFRP. Also, it can be seen that using the resilience–cost of retrofit optimization framework, even if the LCC is not calculated, the most optimal retrofit designs almost have a lower LCC than the status quo (or non-retrofitted bridge network).

In this regard, the resilience–cost of retrofit optimization can lead to a suitable decision-making framework because the performance level of the infrastructure can be directly measured using the resilience index, and the cost of retrofit can help better refine retrofitting designs. However, a significant budget for a retrofit program in a multi-component complex such as a bridge network is needed. Therefore, bridges must be prioritized for retrofitting based on the required budget and time. For this reason, a Resilience–LCC optimization framework is proposed for bridge network management. The final result of Resilience–LCC optimization as Pareto front is depicted in Fig. 12(b).

In Fig. 12(b), the vertical axis indicates the cost (i.e., the LCC for points and the cost of retrofit for bars). Also, the most optimal retrofit strategies for lower bound, upper bound, and the 4–3–3B are presented in Table 8. The findings indicate that to achieve the most effective retrofit strategies, it is crucial to strike a balance between the cost of retrofit and the reduction in total life-cycle repair cost resulting from retrofitting. The timing of the retrofitting is also an essential factor to consider in the overall optimization framework for life-cycle cost. It is evident from the results that steel jacketing is not among the top optimal retrofit strategies due to its higher cost and lesser effectiveness in reducing the total life-cycle repair cost compared to GFRP and CFRP materials. Based on the Resilience–LCC optimization results, the most effective retrofitting approaches involve using CFEP and GFRP materials of medium to high thickness to jacket all the bridge piers during the initial years of the retrofitting program. This is because this approach

Table 8
The most optimal retrofit strategies based on the resilience–LCC optimization framework.

Strategy				LCC ($)	R (%)
Name	Low Seismicity	Medium Seismicity	High Seismicity		
Strategy L1	GA1T2 (0)	GA1T2 (0)	CA1T2 (0)	9,568,799	85.20
Strategy L2	GA1T2 (0)	GA1T2 (0)	GA1T4 (0)	9,690,442	85.82
Strategy L3	GA1T2 (0)	GA1T3 (0)	CA1T2 (0)	9,760,630	86.38
Strategy L4	GA1T2 (0)	GA1T3 (0)	GA1T4 (0)	9,779,533	87.00
Strategy L5	GA1T3 (0)	CA1T2 (0)	GA1T4 (0)	10,007,180	87.77
Strategy L6	GA1T4 (0)	GA1T4 (0)	GA1T4 (0)	10,167,743	88.63
Strategy L7	CA1T3 (0)	CA1T3 (0)	CA1T3 (0)	10,712,656	90.23
Strategy L8	CA1T4 (0)	CA1T4 (0)	CA1T4 (0)	11,795,512	92.20
Strategy H1	GA1T2 (14)	GA1T2 (14)	GA1T2 (14)	11,505,247	83.54
Strategy H2	GA1T2 (14)	GA1T2 (14)	GA1T3 (14)	11,676,144	84.87
Strategy H3	GA1T2 (14)	GA1T2 (14)	GA1T4 (14)	11,731,902	85.82
Strategy H4	GA1T3 (14)	GA1T3 (14)	GA1T3 (14)	12,228,288	86.52
Strategy H5	CA1T2 (14)	CA1T2 (14)	CA1T2 (14)	12,250,519	87.27
Strategy H6	GA1T4 (14)	GA1T4 (14)	GA1T4 (14)	12,694,498	88.63
Strategy H7	CA1T3 (14)	CA1T3 (14)	CA1T3 (14)	13,050,352	90.23
Strategy H8	CA1T4 (14)	CA1T4 (14)	CA1T4 (14)	14,365,732	92.20
Strategy 4–4–3B1	GA1T2	GA1T2	GA1T3	10,727,687	84.87
Strategy 4–4–3B2	GA1T2	GA2T3	CA1T2	10,950,920	85.39
Strategy 4–4–3B3	GA1T2	GA1T3	CA1T2	10,980,749	86.38
Strategy 4–4–3B4	CA1T2	CA1T2	CA1T2	10,999,816	87.27
Strategy 4–4–3B5	GA2T3	CA1T2	CA1T3	11,265,854	88.10
Strategy 4–4–3B6	GA1T4	GA1T4	GA1T4	11,359,705	88.63
Strategy 4–4–3B7	CA1T3	CA1T3	CA1T3	12,170,773	90.23
Strategy 4–4–3B8	CA1T4	CA1T4	CA1T4	13,312,866	92.20s

considers both the functionality/performance and cost-benefit effects simultaneously and directly within this framework. Hence, the determination of the most suitable retrofit approaches considers three key factors: (1) the significance of minimizing the total life-cycle repair cost, (2) the cost of retrofit, and (3) the total life-cycle maintenance cost.

7. Conclusions

This study proposed a logical optimization framework that aims to facilitate decision-making and identify the most effective retrofit strategies for infrastructure management. In this regard, single- and multi-objective optimization frameworks are examined and compared for an illustrative bridge network. The different objectives include the LCC as a single objective optimization, the resilience–cost of retrofit, and the Resilience–LCC as multi-objective optimizations. For this purpose, different retrofit strategies are considered, including three materials (steel, CFRP, and GFRP), four thickness grades (T1 to T4), eight arrangements (A1 to A8), and ten timings of retrofitting actions. Based on the results, specific conclusions are summarized as follows:

- Logical optimization frameworks are suggested to identify the best retrofit strategies that minimize the life-cycle cost (or the cost of retrofit) and maximize the resilience index for the bridge network through the Non-dominated Sorting Genetic Algorithm II.
- Life-cycle cost analysis is conducted under multiple occurrences of seismic hazard, and retrofit strategies include various times, materials, thicknesses, and arrangements.
- The fragility curves are created based on the specific structural and site characteristics. The gap between the calculated fragility value and the damage state severity (from slight to complete) increases with higher seismic intensities, especially for non-retrofitted structures.
- The resilience curves/surfaces demonstrate that choosing an appropriate retrofit design enhances predictability and reliability in the face of uncertainties.
- The total life-cycle maintenance cost is directly related to the combined costs of the bridge's initial value (or the cost of construction) and the cost of retrofit. Based on the R/N ratio, the retrofit actions cause an approximate 3 % increase in this cost.
- The total life-cycle repair cost is controlled by factors such as seismic hazard curve, structural vulnerability, and incurred direct and indirect losses. Additionally, different timings of retrofitting have a crucial role in decreasing the total life-cycle repair cost, with early retrofitting significantly reducing this cost term. The RE ratio demonstrates the positive impact of implementing retrofit in the initial years, but this effect diminishes when the retrofit program is postponed.
- The total life-cycle cost results indicate that each retrofit strategy has a unique impact on reducing or increasing this cost term compared to the non-retrofitted case. It is essential to mention that the retrofit program has the most significant effect in the first years. However, delaying these actions significantly diminishes their effectiveness to the point where they may even raise the LCC. To determine the most optimal retrofit strategies based on the total life-cycle cost criteria, it is essential to balance two critical factors, including reducing the total life-cycle repair cost caused by retrofitting and minimizing the cost of retrofit.
- Through comparing various optimization frameworks such as single-objective optimization (i.e., the LCC), multi-objective optimization 1 (the resilience–cost of retrofit), and multi-objective optimization 2 (the Resilience–LCC), it can be inferred that the proposed LCC-resilience approach provides more comprehensive strategies by taking into account simultaneously both functionality and cost-effectiveness.

Relevance to resilience

Resilience is increasingly becoming a central idea in designing, assessing, monitoring, maintaining, and managing infrastructure systems. Resilience can be defined as the ability of a system to withstand the effects of disruptive events and efficiently recover to pre-event performance. In infrastructure management, decision-makers need to develop disaster risk reduction methodologies to find the most optimal mitigation strategies. In this regard, this research proposes a logical optimization framework by investigating and comparing various objectives, such as resilience and life-cycle cost, through single- or multi-objective optimization. This framework presents a comprehensive understanding of the current and future states of the under-study system, enabling

decision-makers to make informed decisions on how to effectively manage infrastructure throughout its life-cycle.

Compliance with ethical standards

Conflict of interest: The authors declare no conflict of interest.

Replication of results

Detailed information on the proposed methods, simulation models, and software used in this article can be found in the corresponding sections. This includes the algorithms and parameters used. The data that support the findings of this study are available from the first author upon reasonable request.

Author statements and declarations

Author Contributions: All authors contributed to the study conception and design. Material preparation, data collection and analysis were performed by Pedram Omidian, Naser Khaji and Ali Akbar Aghakouchak. All authors read and approved the final manuscript

The authors declare that no funds, grants, or other support were received during the preparation of this manuscript.

Declaration of competing interest

The authors have no relevant financial or non-financial interests to disclose.

CRediT authorship contribution statement

Pedram Omidian: Writing – review & editing, Writing – original draft, Visualization, Validation, Supervision, Software, Resources, Methodology, Investigation, Formal analysis, Data curation, Conceptualization. **Naser Khaji:** Writing – review & editing, Writing – original draft, Visualization, Validation, Supervision, Resources, Methodology, Investigation, Formal analysis, Data curation, Conceptualization. **Ali Akbar Aghakouchak:** Writing – review & editing, Writing – original draft, Visualization, Validation, Supervision, Resources, Methodology, Investigation, Formal analysis, Data curation, Conceptualization.

Acknowledgments

The authors would like to thank anonymous reviewers for their constructive comments, which greatly improved the quality of the initial manuscript.

Appendix A

To validate the accuracy and reliability of the outcomes derived from the modeling conducted via the SeismoStruct software [50], a nonlinear time-history analysis is undertaken. This analysis aims to assess the behavior of an actual RC bridge pier subjected to a uniaxial SGM based on the study conducted by Bianchi et al. [86]. Fig. A1(a) illustrates the actual model installed on the shaking table. The RC bridge pier was designed according to the Caltrans design specifications and criteria [87]. However, it was not based on any existing prototype RC bridge pier. The cantilever RC bridge pier had a diameter of 1.22 m (4 feet) and extended 7.31 m (24 feet) above its footing. With an aspect ratio of six (height to diameter), the test specimen was expected to behave in a nonlinear manner, primarily exhibiting flexural behavior. The column was not straightened or repaired between tests. For longitudinal reinforcement, it featured eighteen 35.8 mm (#11) bars arranged in a single concentric layer. The transverse reinforcement included butt-welded double 15.9 mm (#5) hoops spaced 152 mm (6 inches) apart. The double designation indicates that two hoops were bundled together at each

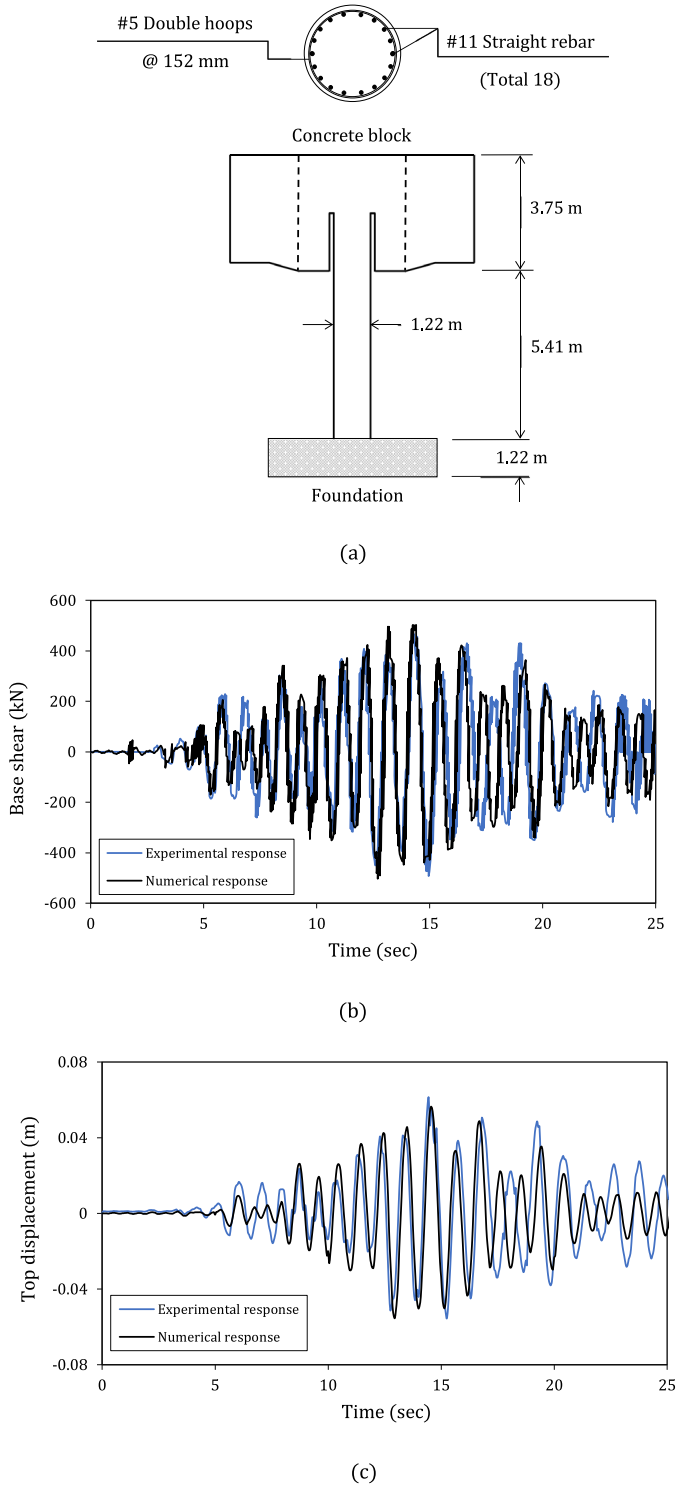

Fig. A1. General view of (a) a full-scale tested reinforced concrete bridge pier [86]. The numerical and experimental (b) base shear and (c) top displacement caused by the seismic record used in Bianchi et al. [86].

152 mm interval. The clear cover of the hoops was 51 mm (2 inches). Fig. A1 illustrates the layout of the column reinforcement and the geometry of the test specimen, consistent with standard bridge construction practices in California; all steel reinforcement met the ASTM A706, Grade 60 specifications. The longitudinal reinforcement ratio of the column was 1.55 %, which is typical of current standards. The transverse reinforcement achieved a volumetric confining ratio of 0.95 %. The reinforcement conformed to Caltrans minimum and maximum specifica-

tions [87]. The estimated axial load at the base of the column was 2.53 MN (570 kips). Considering the concrete strength measured on the first day of testing, this axial load resulted in an axial load ratio of 5.3 %. For model validation, Fig. A1(b-c) compares the responses of base shear and top displacement for the bridge pier simulated using the SeismoStruct and the results obtained from the shaking-table experiment. Obviously, there is a close alignment between the numerically predicted and experimentally measured time-history data for both top displacement and base shear responses.

References

[1] Feng K, Wang C, Li Q. Evaluating the role of transportation system in community seismic resilience. Resilient Cities Struct 2024;3(3):65–78. doi:10.1016/j.rcns.2024.05.003.

[2] Godazgar B, Balomenos GP, Tighe SL. Resilience surface for quantifying hazard resiliency of transportation infrastructure. Resilient Cities Struct 2023;2(3):74–86. doi:10.1016/j.rcns.2023.08.001.

[3] Van De Lindt JW, Kruse J, Cox DT, Gardoni P, Lee JS, Padgett J, McAllister TP, Barbosa A, Cutler H, Van Zandt Sh, Rosenheim N, Navarro CM, Sutley E, Hamideh A. The interdependent networked community resilience modeling environment (IN-CORE). Resilient Cities Struct 2023;2(2):57–66. doi:10.1016/j.rcns.2023.07.004.

[4] Chaudhary RK, Gernay T, Van Coile R. Cost-optimization based target reliabilities for design of structures exposed to fire. Resilient Cities Struct 2024;3(2):20–33. doi:10.1016/j.rcns.2024.03.004.

[5] Omidian P, Khaji N. A total life-cycle cost–resilience optimization framework for infrastructures management using different retrofit strategies. Sustain Resilient Infrastruct 2023;8(6):675–98. doi:10.1080/23789689.2023.2257516.

[6] Wang H, Guo X, Luo Ch, Zhao J, Feng H. Life-cycle cost assessment of the base-isolated-reinforced concrete structure. J Earthquake Tsunami 2024. doi:10.1142/S179343112450026X.

[7] Shekhar Sh, Ghosh J. A metamodeling based seismic life-cycle cost assessment framework for highway bridge structures. Reliabil Eng Syst Saf 2020;195:106724. doi:10.1016/j.ress.2019.106724.

[8] Torti M, Venanzi I, Laflamme S, Ubertini F. Life-cycle management cost analysis of transportation bridges equipped with seismic structural health monitoring systems. Struct Health Monit 2021;21(1):100–17. doi:10.1177/1475921721996624.

[9] Roohi M, Ghasemi S, Sediek O, Jeon H, Van De Lindt JW, Shields M, Hamideh S, Cutler H. Multi-disciplinary seismic resilience modeling for developing mitigation policies and recovery planning. Resilient Cities Struct 2024;3(2):66–84. doi:10.1016/j.rcns.2024.07.003.

[10] Ke S-S, H Ch-H, Yang Ch-Y. Rapid crisis response in resilient cities: emergency response to and reconnaissance of earthquake disasters in Taiwan. J Earthquake Tsunami 2024;18(4):2450008. doi:10.1142/S1793431124500088.

[11] Zhang Y, Ayyub BM, Feng JF, Labe ZM. Incorporating extreme event attribution into climate change adaptation for civil infrastructure: methods, benefits, and research needs. Resilient Cities Struct 2024;3(1):103–13. doi:10.1016/j.rcns.2024.03.002.

[12] Lu J, Atamturktur S, Huang Y. Bi-level resource allocation framework for retrofitting bridges in a transportation network. Transp Res Record: J Transp Res Board 2016;2550(1):31–7. doi:10.3141/2550-05.

[13] Patel DA, Lad VH, Chauhan KA, Patel KA. Development of bridge resilience index using multicriteria decision-making techniques. J Bridge Eng 2020;25(10):04020090. doi:10.1061/(ASCE)BE.1943-5592.0001622.

[14] Rasulo A, Pelle A, Briseghella B, Nuti CA. Resilience-based model for the seismic assessment of the functionality of road networks affected by bridge damage and restoration. Infrastructures (Basel) 2021;6(8):112. doi:10.3390/infrastructures6080112.

[15] Yavuz C. Multi-hazard risk assessment of south Korean nuclear power plants. J Earthquake Tsunami 2023;17(3):2350015. doi:10.1142/S179343112350015X.

[16] Omidian P, Khaji N, Aghakouchck AA. A logical retrofit strategy optimization framework for resiliency bridge infrastructure management considering life-cycle cost. Sustain Struct 2024;4(1):000036. doi:10.54113/j.sust.2024.000036.

[17] Omidian P, Khaji N, Aghakouchck AA. Seismic time-dependent resilience assessment of aging highway bridges incorporating the effect of retrofitting. Structures 2024;63:106347. doi:10.1016/j.istruc.2024.106347.

[18] Satyannarayana R, Rajesh BG. Spatial variation of earthquake hazard for Amaravati city of Peninsular India: a probabilistic approach. J. Earthquake Tsunami 2024;18(6):2450021. doi:10.1142/S1793431124500210.

[19] Omidian P, Khaji N. A multi-objective optimization framework for seismic resilience enhancement of typical existing RC buildings. J Build Eng 2022;52:104361. doi:10.1016/j.jobe.2022.104361.

[20] Deb K, Prata A, Agarwal A, Meyarivan T. A fast and elitist multi-objective genetic algorithm: NSGA-II. IEEE Trans Evol Comput 2002;6(2):182–97. doi:10.1109/4235.996017.

[21] Lewin Ch, Rossi M, Soultani E, Raj KR. Managing infrastructure resilience and adaptation. Sustain Resilient Infrastruct 2023;9(2):107–23. doi:10.1080/23789689.2023.2241728.

[22] Sun J, Bathgate K, Zhang Zh. Bayesian network-based resilience assessment of interdependent infrastructure systems under optimal resource allocation strategies. Resilient Cities Struct 2024;3(2):46–56. doi:10.1016/j.rcns.2024.06.001.

[23] Kim J-S, Park W-S, Han T-S. Framework to evaluate seismic fragility of bridges considering component damage correlations. J Earthquake Tsunami 2021;15(5):2150022. doi:10.1142/S1793431121500226.

[24] Altunişik AC, Sunca F, Sevim B. Ambient vibration-based seismic evaluation of long-span prestressed concrete box-girder bridges under long-duration, near-fault and far-fault ground motions. J Earthquake Tsunami 2024;18(6):2450019. doi:10.1142/S1793431124500192.

[25] HAZUS–MH MR5 Multi-hazard loss estimation methodology–earthquake model. Department of Homeland Security, Washington DC; 2014. Accessed URL: https://www.hsdl.org/c/view?docid=12760 .

[26] Hutt CM, Vahanvaty T, Kourehpaz P. An analytical framework to assess earthquake-induced downtime and model recovery of buildings. Earthquake Spectra 2022;38(2):1283–320. doi:10.1177/8755293021106085.

[27] Fu Zh, Wu D, Fang L, Chen D, Ji B. Influence factors and repair effects of seismic damage to a box section steel pier. J Earthquake Tsunami 2019;13(3–4):1940001. doi:10.1142/S1793431119400013.

[28] Fereshtehnejad H, Shafieezadeh A. A multi-type multi-occurrence hazard lifecycle cost analysis framework for infrastructure management decision making. Eng Struct 2018;167:504–17. doi:10.1016/j.engstruct.2018.04.049.

[29] Yousfi N, Belkacem BA, Guessoum N, Bensaibi M. Seismic resilience scenario of Algerian buildings' context: blida city case study. J Earthquake Tsunami 2024;18(3):2450005. doi:10.1142/S1793431124500052.

[30] Li S-Q. Seismic risk model for regional buildings that considers the influence of temperature and intensity measures. Expert Syst Appl 2024;250:123962. doi:10.1016/j.eswa.2024.123962.

[31] Li S-Q, Zhong J. Development of a seismic vulnerability and risk model for typical bridges considering innovative intensity measures. Eng Struct 2023;302:117431. doi:10.1016/j.engstruct.2023.117431.

[32] Li S-Q, Gardoni P. Optimized seismic hazard and structural vulnerability model considering macroseismic intensity measures. Reliab Eng Syst Saf 2024;252:110460. doi:10.1016/j.ress.2024.110460.

[33] Li S-Q. Hybrid seismic vulnerability models for regional structures considering bivariate intensity measures. Soil Dyn Earthquake Eng 2024;183:108763. doi:10.1016/j.soildyn.2024.108763.

[34] Aristeidou S, O'Reilly GJ. Exploring the use of orientation-independent inelastic spectral displacements in the seismic assessment of bridges. J Earthquake Eng 2024;28(12):3515–38. doi:10.1080/13632469.2024.2343067.

[35] Xie Y, Zhang J, Desroches R, Padgett JE. Seismic fragilities of single-column highway bridges with rocking column-footing. *Earthquake Eng* Struct Dyn 2019;48(7):843–64. doi:10.1002/eqe.3164.

[36] Fakharifar M, Chen G, Sneed L, Dalvand A. Seismic performance of post-mainshock FRP/steel repaired RC bridge columns subjected to aftershocks. Compos Part B: Eng 2015;72:183–98. doi:10.1016/j.compositesb.2014.12.010.

[37] Uenaga T, Omidian P, George RC, Mirzajani M, Khaji N. Seismic resilience assessment of curved reinforced concrete bridge piers through seismic fragility curves considering short- and long-period earthquakes. Sustainability 2023;15(10):7764. doi:10.3390/su15107764.

[38] Padgett JE, DesRoches R. Methodology for the development of analytical fragility curves for retrofitted bridges. Earthquake Eng Struct Dyn 2008;37(8):1157–74. doi:10.1002/eqe.801.

[39] Oregon highways seismic plus. (2014). ODOT's oregon highways seismic plus report, bridge and geo-environmental sections, Oregon department of transportation. Accessed URL: https://www.oregon.gov/odot/Bridge/Docs_Seismic/Seismic-Plus-Report_2014.pdf>.

[40] ISMEP. (2014). Istanbul seismic risk mitigation and emergency preparedness project (ISMEP), No.4 retrofitting and reconstruction works, 1–96, June 2014, Beyaz Gemi Social Project Agency. Accessed URL: https://www.ipkb.gov.tr/wp-content/uploads/2019/07/ISMEP4_GUCLENDIRME_EN140214.pdf.

[41] Washington state's bridge seismic retrofit program. (2019). WSDOT's bridge seismic retrofit program and bridge resiliency assessment Data, the Washington State Department of Transportation. Accessed URL: https://publications.anl.gov/anlpubs/2020/01/157924.pdf>.

[42] Kabir MR, Muntasi Billah AHM, Shahria Alam M. Seismic fragility assessment of a multi-span RC bridge in Bangladesh considering near-fault, far-field and long duration ground motions. Structures 2019;19:333–48. doi:10.1016/j.istruc.2019.01.021.

[43] Speranza E, De Martino G, Conte Ch, Dolce M. Italian national seismic prevention plan: cost analyses for risk reduction policies. Procedia Struct Integr 2023;44:1784–91. doi:10.1016/j.prostr.2023.01.228.

[44] Du A, Padgett JE, Shafieezadeh A. Adaptive IMs for improved seismic demand modeling of highway bridge portfolios. Los Angeles, CA, USA: Proceedings of the 11th National Conference in Earthquake Engineering; 2018. 25–29 June 2018.

[45] Raghunandan M, Liel AB, Luco N. Aftershock collapse vulnerability assessment of reinforced concrete frame structures. Earthquake Eng Struct Dyn 2015;44(3):419–39. doi:10.1002/eqe.2478.

[46] Naseem A, Kashif M, Schotte K, Backer HD. Seismic fragility curves of combined multiple tunnel complexes in soft soils. J Earthquake Tsunami 2023;17(6):2350026. doi:10.1142/S1793431123500264.

[47] Liang Y, Kong Y-Zh, Zhao Ch-X, Liu R-Q, Luo J, Zhu RH. Time-varying seismic fragility analysis of ECC-RC composite bridge with high-strength steel bars. J Earthquake Tsunami 2024;18(1):2350029. doi:10.1142/S179343112350029X.

[48] Yaghmaei-Sabegh S, Neekmanesh Sh. Non-parametric seismic fragility curves of SDOF systems based on a clustering process. J Earthquake Tsunami 2023;17(3):2350008. doi:10.1142/S1793431123500082.

[49] Sultan, M., Kawashima, K. (1993). Comparison of the seismic design of highway bridges in California and in Japan," Recent selected publications of Earthquake Engineering Div., Public Works Research Institute (PWRI), Japan (Technical Memorandum of PWRI No. 3276). Accessed URL: https://thesis.pwri.go.jp/public_detail/109658/.

[50] SeismoStruct. (2024). SeismoSoft, A computer program for static and dynamic nonlinear analysis of framed structures. Accessed URL: https://seismosoft.com/product/seismostruct/
[51] Madas P, Elnashai AS. A new passive confinement model for the analysis of concrete structures subjected to cyclic and transient dynamic loading. Earthquake Eng Struct Dyn 1992;21:409–31. doi:10.1002/eqe.4290210503.
[52] Mander JB, Priestley MJN, Park R. Theoretical stress-strain model for confined concrete. J Struct Eng 1988;30:1804–26. doi:10.1061/(ASCE)0733-9445(1988)114:8(1804.
[53] Martinez-Rueda JE, Elnashai AS. Confined concrete model under cyclic load. Mater Struct 1997;30:139–47. doi:10.1007/BF02486385.
[54] Yassin MHN. Nonlinear analysis of prestressed concrete structures under monotonic and cyclic loads, Berkeley, USA: PhD Thesis, University of California; 1994. Accessed URL: https://search.worldcat.org/en/title/222312210 .
[55] Filippou, F.C., Popov, E.P., Bertero, V.V. (1983). Effects of bond deterioration on hysteretic behaviour of reinforced concrete joints, Report EERC 83-19, Earthquake Engineering Research Center, University of California, Berkeley, USA. Accessed URL: https://nehrpsearch.nist.gov/static/files/NSF/PB84192020.pdf.
[56] Monti, G., Nuti, C., Santini, S. (1996). CYRUS -cyclic response of upgraded sections, Report No. 96-2, University of Chieti, Italy. Accessed URL: https://hdl.handle.net/11590/191035.
[57] Fragiadakis M, Pinho R, Antoniou S. Modelling inelastic buckling of reinforcing bars under earthquake loading. Book: computational structural dynamics and earthquake engineering: structures and infrastructures book series, 2. 1st ed. CRC Press; 2008. doi:10.1201/9780203881637.
[58] FIB (Fédération International du Béton). (2006). Retrofitting of concrete structures by externally bonded FRPS, with emphasis on seismic applications, FIB Bulletin No. 35, Federation Internationale du Beton, 220. DOI: 10.35789/fib.BULL.0035
[59] Ferracuti B, Savoia M. Cyclic behavior of CFRP-wrapped piers under axial and flexural loading. In: Proceedings of the International Conference on Fracture, Turin, Italy; 2005. Accessed URL: https://citeseerx.ist.psu.edu/document?repid=rep1&type=pdf&doi=8b61f15de5c256d85fbf9eb8e8e02d4d1872aa33 .
[60] Spoelstra MR, Monti G. FRP-confined concrete model. J Compos Construct 1999;3:143–50. doi:10.1061/(ASCE)1090-0268(1999)3:3(143.
[61] Yankelevsky DZ, Reinhardt HW. Uniaxial behavior of concrete in cyclic tension. J Struct Eng 1989;115:166–82. doi:10.1061/(ASCE)0733-9445(1989)115:1(166.
[62] Choi E. Seismic analysis and retrofit of Mid-America bridges, USA: PhD Thesis, Georgia Institute of Technology; 2002. Accessed URL: https://www.researchgate.net/deref/http%3A%2F%2Fhdl.handle.net%2F1853%2F21538?_tp=eyJjb250ZXh0Ijp7ImZpcnN0UGFnZSI6InB1YmxpY2F0aW9uIiwicGFnZSI6InB1YmxpY2F0aW9uIiwicG9zaXRpb24iOiJwYWdlSGVhZGVyIn19 .
[63] Maroney B, Kutter B, Romstad K, Chai YH, Vanderbilt E. Interpretation of large scale bridge abutment test results. In: Proceedings of 3rd Annual Seismic Research Workshop, California Department of Transportation, CA, June 27-29; 1994.
[64] Caltrans. (2013). Seismic design criteria version 1.7, California department of transportation. Accessed URL: https://dot.ca.gov/-/media/dot-media/programs/engineering/documents/seismicdesigncriteria-sdc/f0006116-justification-of-caltrans-seismic-design-criteria-sdc-1.pdf.
[65] Muthukumar S, DesRoches R. A Hertz contact model with non-linear damping for pounding simulation. Earthquake Eng Struct Dyn 2006;35(7):811–28. doi:10.1002/eqe.557.
[66] Omidian P, Saffari H. Comparative analysis of seismic behavior of RC buildings with shape memory alloy rebar in regular, torsional irregularity and extreme torsional irregularity cases. J Build Eng 2018;20:723–53. doi:10.1016/j.jobe.2018.09.020.
[67] Shome, N., Cornel, C.A. (1999). Probabilistic seismic demand analysis of nonlinear structures, Reliability of Marine Structures Program Technical Report RMS-35, Stanford Digital Repository. Accessed URL: https://purl.stanford.edu/qp089qb1141.
[68] PEER. (2024). Pacific earthquake engineering research center, PEER, online strong motion database. Accessed URL: https://ngawest2.berkeley.edu/
[69] Abbasi M, Zakeri B, Amiri GG. Probabilistic seismic assessment of multiframe concrete box-girder bridges with unequal-height piers. J Perform Construct Facil 2015;30(2):04015016. doi:10.1061/(asce)cf.1943-5509.0000753.
[70] Petersen, M.D., Frankel, A.D., Harmsen, S.C., Mueller, C.S., Haller, K.M., Wheeler, R.L., Wesson, R.L., Zeng, Y., Boyd, O.S., Perkins, D.M., Luco, N., Field, E.H., Wills, C.J., Rukstales, S. (2008). Documentation for the 2008 update of the united states national seismic hazard maps, U.S. Geological Survey (USGS) Open-File Report 2008–1128, U.S. Geological Survey, Reston, VA. DOI: 10.3133/ofr20081128
[71] Caltrans. (2005). Historic bridge inventory, sample plans of actions. Division of Maintenance, Structure Maintenance. Accessed URL: http://www.dot.ca.gov/hq/structur/strmaint/poa_samp.pdf>.
[72] Calvi GM, O'reilly GJ, Andreotti G. Towards a practical loss-based design approach and procedure. Earthquake Eng Struct Dyn 2021;50(14):3741–53. doi:10.1002/eqe.3530.
[73] Abarca A, Monteiro R, O'reilly GJ. Simplified methodology for indirect loss–based prioritization in roadway bridge network risk assessment. Int J Disaster Risk Reduct 2022;74:102948. doi:10.1016/j.ijdrr.2022.102948.
[74] Soliman M, Frangopol DM. Life-cycle cost evaluation of conventional and corrosion resistant steel for bridges. J Bridge Eng 2014;20(1):06014005. doi:10.1061/(ASCE)BE.1943-5592.0000647.
[75] Gallivan, F., Ang-Olson, J., Papson, A., Venner, M. (2010). Greenhouse gas mitigation measures for transportation construction, maintenance, and operations activities. San Francisco: AASHTO Standing Committee on the Environment. Accessed URL: http://onlinepubs.trb.org/onlinepubs/nchrp/docs/NCHRP25-25(58)_FR.pdf.
[76] Kendall A, Keoleian GA, Helfand GE. Integrated life-cycle assessment and life-cycle cost analysis model for concrete bridge deck applications. J Infrastruct Syst 2008;14(3):214–22. doi:10.1061/(ASCE)1076-0342(2008)14:3(214.
[77] CaltransAnnual average daily truck traffic on the California state highway system. Traffic Data Branch 2016. Accessed URL: https://dot.ca.gov/-/media/dot-media/programs/traffic-operations/documents/census/f0017681-2016-aadt-truck-a11y.pdf .
[78] Abarca A, Monterio R, O'reilly GJ. Seismic risk prioritisation schemes for reinforced concrete bridge portfolios. Struct Infrastruct Eng 2023:1–21. doi:10.1080/15732479.2023.2187424.
[79] Fereshtehnejad E, Hur J, Shafieezadeh A, Brokaw M. Ohio bridge condition index: multilevel cost-based performance index for bridge systems. Transp Res Record: J Transp Res Board 2017;2612(1):152–60. doi:10.3141/2612-17.
[80] Bocchini P, Frangopol DM. Optimal resilience- and cost-based postdisaster intervention prioritization for bridges along a highway segment. J Bridge Eng 2010;17(1):117–29. doi:10.1061/(ASCE)BE.1943-5592.0000201.
[81] ODOT. (2010). Ohio Department of Transportation, Innovative contracting manual, Division of Construction Management. Accessed URL: https://www.dot.state.oh.us/Divisions/ConstructionMgt/Admin/Innovative%20Contracting/Innovative_Contracting_Manual.PDF
[82] Porter K, Shoaf K, Seligson H. Value of injuries in the Northridge earthquake. Earthquake Spectra 2006;22(2):555–63. doi:10.1193/1.2194529.
[83] Caltrans. (2011). High occupancy vehicle lanes status report. Sacramento metropolitan area. District 3. Office of Freeway Operations, Sacramento. Accessed URL: https://dot.ca.gov/programs/traffic-operations/hov
[84] Nims, D.K., Miranda, E., Aiken, I.D., Whttaker, A.S., & Bereto, V.V. (1989). Collapse of the cypress street viaduct as a result of the Loma Prieta earthquake. Earthquake Engineering Research Center, University of California, Berkeley, CA. Accessed URL: 10.13140/RG.2.1.4863.1924
[85] Kliesen, K.L., Mill, J.S. (1994). The economics of natural disasters. The regional economist. Federal Reserve Bank of St. Louis, p. 332. Accessed URL: https://www.stlouisfed.org/publications/regional-economist/april-1994/the-economics-of-natural-disasters.
[86] Bianchi F, Sousa R, Pinho R. Blind prediction of a full-scale RC bridge column tested under dynamic conditions. In: Proceedings of 3rd International Conference on Computational Methods in Structural Dynamics and Earthquake Engineering, COMPDYN 2011; 2011. Paper no. 294, Corfu, Greece. Accessed URL: http://congress.cimne.com/eccomas/proceedings/compdyn2011/compdyn2011_full/294.pdf .
[87] Caltrans Bridge design practices. California Department of Transportation; 2004. Accessed URL: https://dot.ca.gov/programs/engineering-services/manuals/bridge-design-practice .